Structure analysis of self-assembly molecules

Department of Biophysical Engineering
Faculty of Engineering Science
Osaka University

Iwasaki Kenji

March, 1998

Structure analysis of self-assembly molecules

Department of Biophysical Engineering
Faculty of Engineering Science
Osaka University

Iwasaki Kenji

March, 1998

TABLE OF CONTENT

GENERAL INTRODUCTION

In life on Earth, a self-assembly system is widely used for functional macromolecules such as ribosomes as well as living organisms like viruses (Bajaj, 1984; Klug, 1983; Metzler, 1977). Inter cellar interactions in invertebrates, vertebrates and also plant are owing to these self-assembly of proteins. By using the self-assembly, the life takes benefits as following; i) the amount of genetic information is reduced by using some repeating units to construct larger building block. ii) The process of the assembly makes life a lot of chance to repair errors occurred in the constructions. However, the details of the mechanism of self-assembly are still unclear. Now, the most important problem are structure analysis of each component and a whole construction in three-dimension.

In this thesis, two kinds of molecules were examined from such a point of view. Firstly, the three-dimensional structure of integrin αIIbβ3 was studied using a simple-back projection algorithm. Integrins have a critical roll in connecting inner cell and extracellular matrix (Loftus, 1994). αIIbβ3, as representative in this family (Phillips, 1991), exists in platelet, and mediates platelet aggregation through fibrinogen. The three-dimensional structure showed that αIIbβ3 consists of two tails and the head with three novel structures, one of which suggests the binding site to fibrinogen.

Second, a virus capsid protein was studied as an example of the self-assembly of the homologous molecules. Closed structures, which can be seen in virus structures, are favored with stable structures (Harrison, 1984; Harisson, 1992; Hogle, 1987; Rossmann, 1989). For example, sheets

composed of hexagonal arrays are observed. However, a sheet is changed into a tube by a rearrangement of each subunit. A phenomenon like this was observed in a capsid protein of Rice Dwarf Virus (RDV). This capsid protein, P8, usually forms an outer shell of an icosahedral virus particle. However, purified P8 proteins form a slender sheet or tubular crystal in distilled water. This assembly also become a good model for investigating construction in viral replication, because capsid proteins must change contacts and its arrangement depending on situation. Since virus particles must export nucleic acids for replication, they need rearrangements of capsid proteins. In the case of P8, a trimer of P8 functions as a unit. The reconstructed three-dimensional structure of the tubular crystal at 9 Å showed that trimers side by side twisted like a propeller. The trimer itself is composed of two parts, one of which suggests trimer-trimer interface, and another suggests monomer-monomer interface and a relation to infectious function.

Electron microscopy is an appropriate method to examine the structure of one molecule and tubular crystals. I demonstrated novel structures of these materials above-mentioned, which were obtained using an electron microscope and programs developed for an electronmicrograph. The results, including such novel structures, in this thesis could be available to lead general principle for self-assembly systems.

References

Bajaj, M.& Blundell, T. (1984). Evolution and the tertiary structure of proteins. *Annu. Rev. Biophys. Bioeng.* **13**, 453-492

Klug, A. (1983). From macromolecules to biological assemblies. *Biosci, Rep.* **3**, 395-430.

Metzler, D. E. (1977). *Biochemistry.* New York, Academic Press.

Harrison, S. C. (1984). Multiple modes of subunit association in the structures of simple spherical viruses. *Trends Biochem. Sci.* **9**, 345-351.

Harrison, S. C. (1992). Viruses. *Curr. Opin. Struc. Biol.* **2**, 293-299.

Hogle, J. M., Chow, M., Filman, D. J. (1987). The structure of polio virus. *Sci. Am.* **256**, 42-49.

Rossmann, M. G., Johnson, J. E. (1989). Icosahedral RNA virus structure. *Annu. Rev. Biochem.* **58**, 533-573.

Loftus, J. C., Smith, J. W. & Ginsberg, M. H. (1994). Integrin-mediated cell adhesion: The extracellular face. *J. Biol. Chem.* **269**, 25235-25238.

Phillips, D. R., Charo, I. F. & Scarborough, R. M. (1991). GPIIb-GPIIIa: The responsive integrin. *Cell.* **65**, 359-362.

CHAPTER I

Three-dimensional Reconstruction of Integrin $\alpha_{IIb}\beta_3$

I-1 SUMMARY

The three-dimensional structure of a heterodimeric membrane protein, integrin $\alpha_{IIb}\beta_3$, which is a cell adhesion receptor that binds fibrinogen, von Willebrand factor, and fibronectin, was reconstructed from a single-axis tilt series of images of negatively stained specimens. The $\alpha_{IIb}\beta_3$ protein, which was purified from cultured human erythrocyte leukemia cells, exhibited a novel structure. While $\alpha_{IIb}\beta_3$ was composed of an oblong head and two tails, as previously shown, the multi-domain structure of the head was revealed from the reconstructed images.

I-2 INTRODUCTION

Integrins are transmembrane receptors that interact with the extracellular matrix. A portion of the cytoplasmic region of the integrin interacts with the cytoskeleton. This interaction is related to the communication between the cytoskeleton and the extracellular matrix. The $\alpha_{IIb}\beta_3$ integrin is prototypical, and is highly expressed in platelets. This receptor mediates platelet aggregation through binding to a specific tripeptide sequence,

Arg-Gly-Asp (RGD), of fibrinogen. The RGD sequence is also found in other ligands, von Willebrand factor, and fibronectin. Like other members of the integrin family, $\alpha_{IIb}\beta_3$ (*Mr*= 235,000) is composed of two distinct polypeptide chains, called α and β. The structure of $\alpha_{IIb}\beta_3$ has been extensively studied by electron microscopy of isolated receptors, but it has been discussed only from projections that mainly used the rotary shadowing technique [4-5]. Here, we report the 3D structure of $\alpha_{IIb}\beta_3$, reconstructed from micrographs of a single-axis tilt series of negatively stained specimens, and describe a novel structure found in the 3D images.

I-3 MATERIALS AND METHODS

Purification of $\alpha_{IIb}\beta_3$

The $\alpha_{IIb}\beta_3$ integrin is highly expressed in the human erythrocyte leukemia cell line, HEL. The membrane proteins were extracted by incubating HEL cells with a 1% Triton X-100 solution [1], and the $\alpha_{IIb}\beta_3$ protein was purified by sequential chromatography on columns of HiTrap Heparin, Con A-Sepharose, and GRGDSPK-Sepharose [2].

Electron microscopy

A solution of purified $\alpha_{IIb}\beta_3$ (0.5mg/ml, 2μl) was stained with an equal volume of 2% uranyl acetate for 30sec, and was examined in a transmission electron microscope (JEM-1010, JEOL). Images of the single-axis tilt series were collected in a tilt angle range from -55° to +55° in 5° increments. The direct magnification of these images was ×50,000.

I-4 RESULTS

Three sets of integrin molecule images were extracted from the micrographs of one tilt series, in which the particles observed on the grid were almost exclusively in the same orientation to the surface of the carbon support (Fig. 1). Each molecule was boxed out and reconstructed using a simple back-projection algorithm [3]. The surface representations were calculated from the volume of the molecular mass, assuming a protein density of $1.37 g/cm^3$.

In agreement with previous studies that used rotary shadowing [4-5], the images of the negatively stained $\alpha_{IIb}\beta_3$ protein show that many particles appeared to consist of head and tail domains (Fig. 1). There is an oblong head, from which the two tails extend in almost the same direction. The two-domain structure is also clear in the sections of the reconstructed 3D structure, shown in Fig. 2. Their shapes are very similar to each other, although the density at one of the tails was lost in *II,* and in the case of *III*, the part near the head-tail junction was diminished. This is shown in the superimposed surface representations (Fig. 4). One of the two tails found in each integrin molecule is thicker than the other. Only in *I*, the slender tail was found to have a continuous density. However, the dissociated density of the slender tail of *III* corresponded to that of *I* very well. The tip

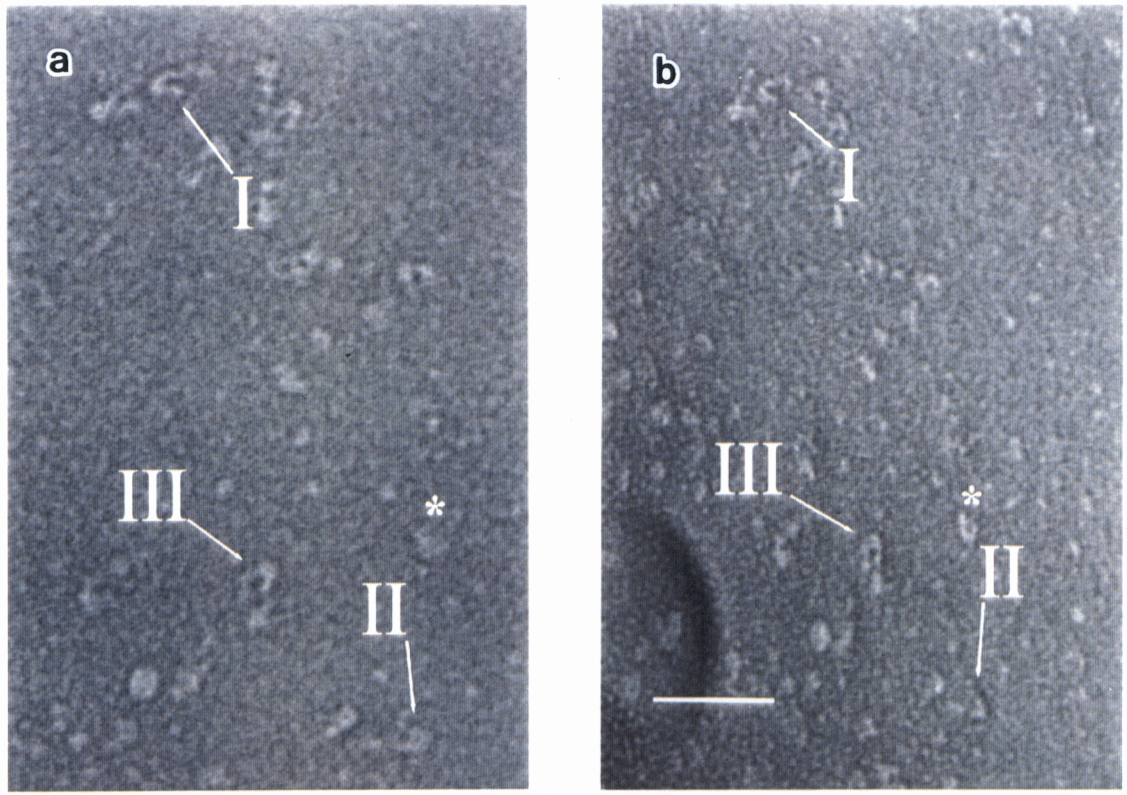

Fig. 1. Electron micrograph of negatively stained αIIbβ3. (*a*) Portion of a micrograph recorded with the specimen grid not tilted. A 512Å×512Å area was selected for the reconstructions. (*b*) The same specimen field as in (a), except with the grid tilted by 55°. Three of the same particles are labeled as I, II, and III. The particle indicated by * has an obscured shape in the nontilted image (a), but the globular head and tails can be seen clearly in the tilted image (b). Bar, 50nm.

a
b
c
d
e
f
g
h
i
j
k
l

Fig. 2. Surface representations of the three particles labeled in Fig. 1. Different views of each particle. The top row, (a), (b), (c), and (d), is particle I. The middle row, (e), (f), (g) and (h) is particle II, and the bottom row, (i), (j), (k), and (l), is particle III. Different views of the same particle are related by a 90° rotation in the vertical direction of this figure. Arrows in (b), (f), and (j) point to the "hornlike domain", the density of which protrudes from the head part of the integrin molecule. Arrows in (a), (g), and (i) show the two lumps on the head. Bar, 10nm.

of the slender tail of *II* appeared to have the same orientation as the other slender tails. The section of the 3D image (Fig. 3) clearly shows that the tip of the slender tail connected to another domain is separated by a section with very low density. As reported from studies of rotary shadowed specimens [4-5], three forms of the tail portion, including this "distal island", were observed. In the first form, the tails are parallel, in the second, they are splayed, and in the third, they touch each other at their ends. The analyzed structures, which are represented in I, II, and III, include all three of these typical forms. The first, second, and third forms are observed in I, II, and III, respectively. However, the intensity of the distal island was too weak to emerge in the reconstructions.

The structures of the globular heads of these reconstructed molecules are similar to each other. It is clear that they have lumps at the top left and the bottom right in the globular head, as shown in Fig. 4 *(a)*. Moreover, the density that protrudes at the opposite side of the lumps looks like a horn. This feature had never been identified before from the projected images produced by the studies of rotary shadowed specimens. Our 3D structures reconstructed from the micrographs of a single-tilt series show that $\alpha_{IIb}\beta_3$ has a globular head with two lumps, the "hornlike" protrusion, and two tails, a slender one, and a thick one. Since we used a single-tilt series for the 3D reconstruction, the theoretical maximum resolutions are approximately 2nm parallel to the tilt axis and 12nm normal to the carbon support [3].

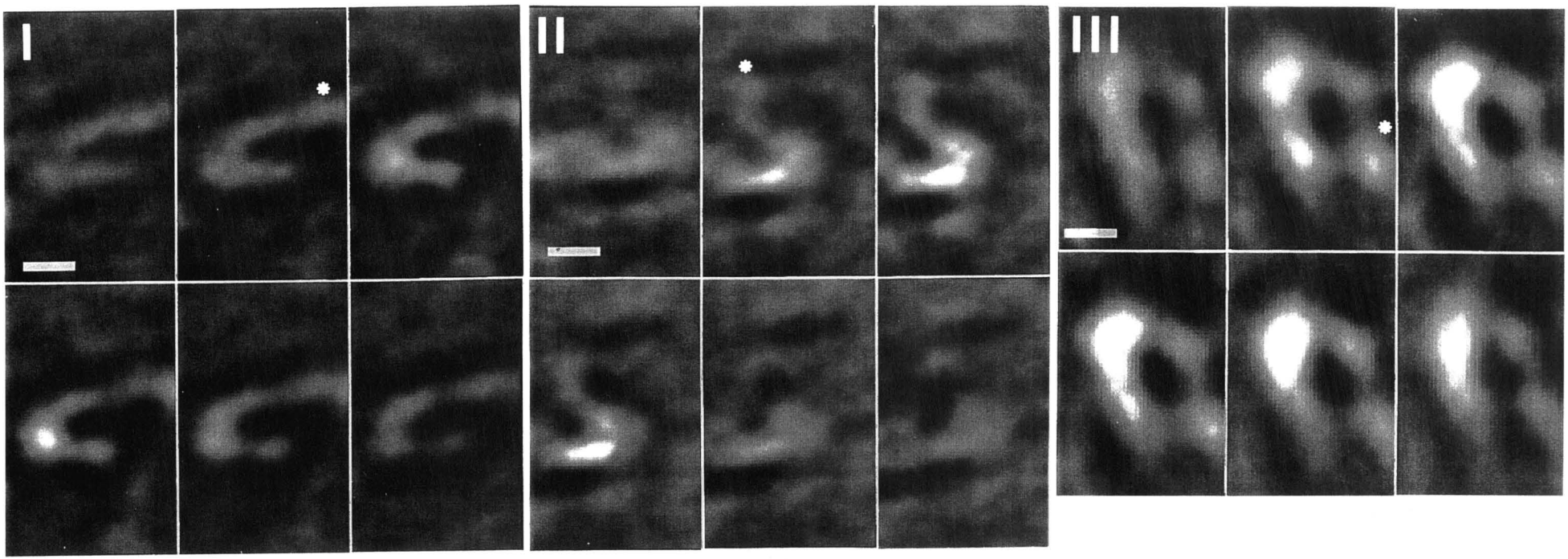

Fig. 3. Sections of three reconstructed $\alpha_{IIb}\beta_3$ particles-I (a), -II (b), and –III (c), respectively. The section plane is parallel to the carbon film and is spaced at 2-nm intervals. The small domain (*) is connected to the tip of the slender tail, which might be a light chain of $\alpha_{IIb}\beta_3$. Bar, 5nm.

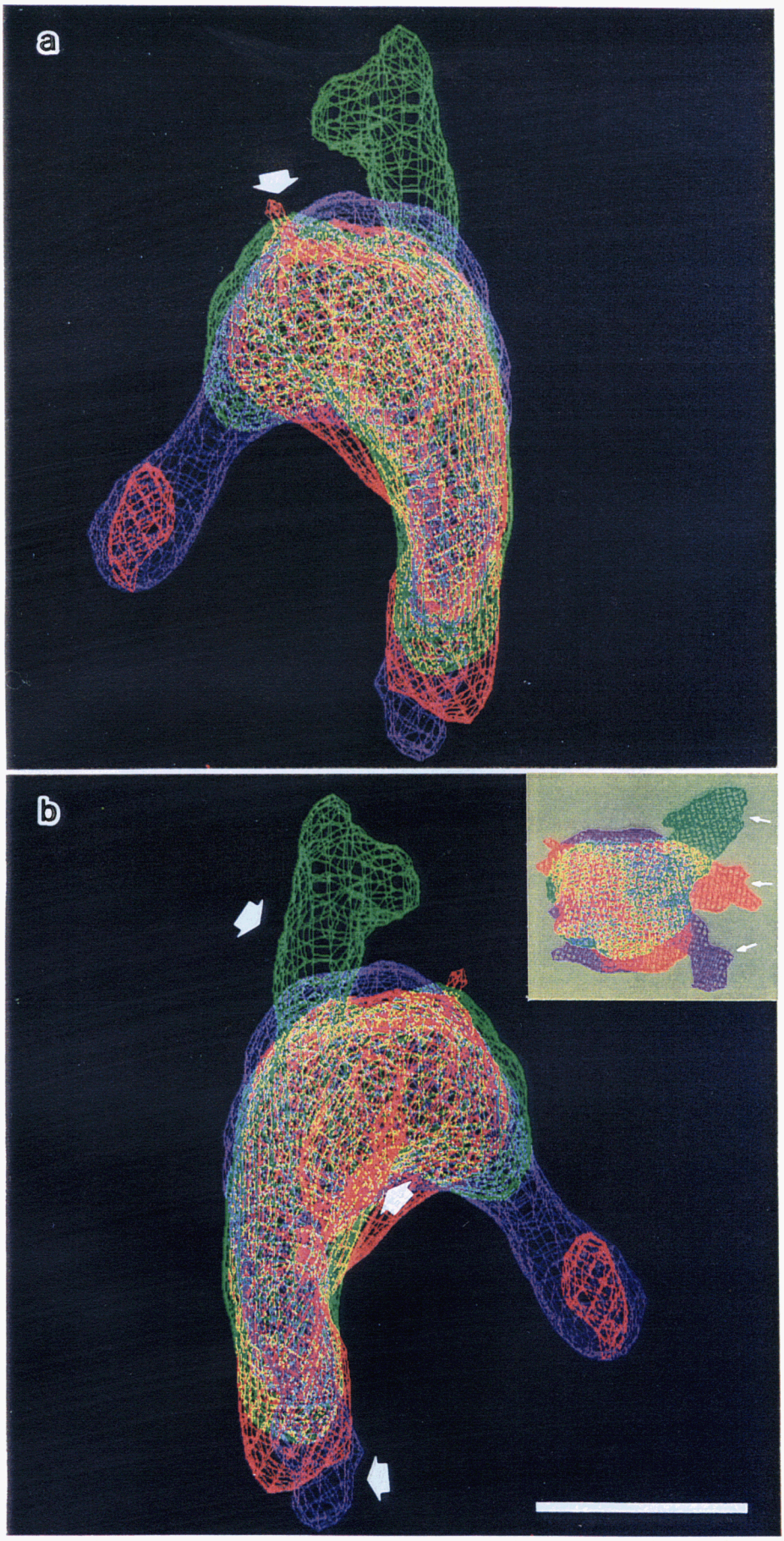

Fig. 4. Superimposed surface representations. (*a*) (a), (g), and (i), from Fig. 2. are superimposed. One of the lumps, indicated by the arrow might be near the binding site of fibrinogen. (*b*) The opposite side of (a). The "hornlike domain" is indicated by the arrow. The entire structure was stretched in the horizontal direction in this figure, because sufficient data were lacking due to the missing wedge. The inset shows a side view of (b). Bar, 5nm.

I-5 DISCUSSION

The anisotropic resolution might affect the shape of the horn-like domain and the wide tail; that is, these domains might be extended toward the direction normal to the carbon support. Nevertheless, it is quite convincing that there is a density at the position where the horn-like domain was observed.

As reported for the rotary shadowed electron micrographs, a globular particle, in addition to the particle with the head and the tails, was observed [5]. The tails of the globular particles had been considered to wrap around the head, due to the flexibility of the tails. However, the two tails emerged in the majority of such particles when the specimen was tilted, suggesting that the tails do not form various conformations, but that the entire particle has a different shape, depending on the direction of the view. Therefore, although previous papers had suggested that the tails are flexible, the result of the tilted image, as well as the agreement among the reconstructed 3D-structures, suggests that the tails have a rather rigid structure.

Comparing a pair of tails in each particle, one of the tails is more slender than the other. Presumably because these parts have less void volume to exclude the stain, and the detergent, which was used for the membrane extraction, interrupts the staining, especially at the hydrophobic transmembrane region of the tails. More importantly, the difference in the tail densities can be attributed to the heterogeneity of the subunits, because α_{IIb} consists of two disulfide-linked subunits , an *Mr*125,000 heavy chain and an *Mr*23,000 light chain [6-7];thus, the shorter tail might be α_{IIb}. This hypothesis is supported by the result that the very low density domain is

connected to the tip of the slender tail and is excluded from the reconstructions (Fig. 3). If this domain corresponds to the light chain of α_{IIb}, then its void volume would be very small and would include the hydrophobic transmembrane region surrounded by detergent molecules. Thus, it is consistent with the hypothesis that the tail with the low density is α_{IIb}, and the other, with the clearly formed shape, is β_3.

In this experiment, two novel integrin structures were found: the two lumps on the head and the horn-like domain extending from the opposite face of the head region (Fig. 3). The angle of the horn-like domain differed among the particles, but this might be a small deformation caused by sample adhesion to the carbon film. The existence of the horn-like domain is verified from the fact that molecule *II* adhered to the carbon in the opposite direction, but shows the horn-like domain at the position near that of the other particles when they are superimposed (Fig. 4). On the other hand, the two lumps are seen on the opposite face of the head. The one located near the shorter tail is a little sharper than the other. This might be related to a ligand-binding site. As previously shown [5], fibrinogen binds to the lateral aspect of the head of $\alpha_{IIb}\beta_3$. The aspect is the side of the head near the tail, with the tip pointed up, and therefore corresponds to the head portion near the shorter tail in the reconstructions. The sharper lump is located near this position. Therefore, it could be a candidate for the fibrinogen binding site.

I-6 ACHKNOWLEDGEMENTS

I would like to thank Takao Yamada for teaching how to purify $\alpha_{IIb}\beta_3$ and sending some materials to me. I am grateful to Dr. Kaoru Mitsuoka for helping image analysis.

I-7 REFERENCES

1 Fitzgerald L A, Leung B and Phillips D R (1985) *Anal. Biochem.* **151**: 169-177

2 Yamada T, Uyeda A, Kidera A and Kikuchi M (1994) *Biochemistry*. **33**: 11678-11683

3 Frank J (1992) *ELECTRON TOMOGRAPHY*. (Plenum Press, New York).

4 Nadia A C, Laurance A F, Beat S, Harold P E and David R P (1985) *J. Biol. Chem*. **260**: 1743-1749

5 John W W, Chandrasekaran N, Gaston V and Joel S B (1992) *J. Biol. Chem.* **267**: 16637-16643

6 Jennings L K and Phillips D R (1982) *J.Biol.Chem.* **257**: 10458-10466

7 Juan J C, Maria V A, Germán R, Choy-L H, Agnes H and José G R *Biochem. J.* **261**: 551-560

CHAPTER II-1

Details of the arrangement of the outer capsid of rice dwarf phytoreovirus, as visualized by two-dimensional crystallography

II-1.1 SUMMARY

Two-dimensional crystals were obtained from purified P8, an outer capsid protein of rice dwarf phytoreovirus. A filtered image of the two-dimensional crystal, in combination with the results of biochemical analysis, revealed the unit formation of the capsid protein, a capsomere structure, which appeared to be an approximately equilateral triangle with sides of approximately 6nm and which was composed of a trimer of P8 protein. Details of the arrangements of the outer capsid of the virus are described.

II-1.2 INTRODUCTION

Rice dwarf virus (RDV) belongs to a phytoreovirus genus that is a member of the family *Reoviridae* (Holmes *et al.*, 1995). It is transmitted to rice and wheat plant by *Nephotettix* speciese and causes stunting or

dwarfing of plant bodies. The phytoreoviruses are able to replicate in both plants and insects. But its mechanism has not been elucidated clearly.

The 12 segments of double-stranded RNA (Omura & Inoue, 1985) and seven proteins (Nakata *et al.*, 1978) form the icosahedral double-shelled particles. The diameter of the intact virus particle is about 70nm and that of the core particle is about 53nm. (Kimura & Shikata, 1968; Uyeda & Shikata, 1982).

The eight largest (S8) of the 12 genome segments of RDV encodes a polypeptide of 420 amino acids with an *Mr* of 46422 (Omura *et al.*, 1989). This protein, named P8, conseved in other phytoreoviruses which are wound tumor virus (WTV) and rice gall dwarf virus (RGDV) and forms part of the outer capsid in all of these viruses (Noda *et al.*, 1991; Takahashi *et al.*, 1994; Xu *et al.*, 1989; Reddy *et al.*, 1976; Omura *et al.*, 1985; Omura *et al.*, 1989). Morerevor, the outer capsid protein P8 has the highest homology (48-56% amino acid identity) among the nucleotide sequences of corresponding segments of the three viruruses. This may relates to almost identical morphology of these viruses, which was observed by electron microscopy (Streissle *et al.*, 1968; Omura *et al.*, 1989; Omura & Inoue, 1985; Boccard *et al.*, 1985). In the case of these viruses, some parts in amino acid homorogous regions of P8 may contact with core capsid proteins (Noda *et al.*, 1991). Furtheremore, core particles and outer capsids were interchangeable between these viruses. The outer shell of RDV is composed of 260 capsomeres (Lu *et al.*, 1995) and the fact that the weight of the unit capsomere is 138.5kDa suggests that the one capsomere composes of three molecules of P8 proteins (Omura *et al.*, 1989).

There is also a P2 minor outer capsid protein besides the P8 major outer

capsid protein in the outer capsid layer. While the P2 minor outer capsid protein was recently shown to be esential for infection (Yan *et al.*, 1996), the P8 major outer capsid protein also appears to be associated with infection because neutralizing antibodies can be raised against this protein (Omura, Unpublished). Moreover, the appearances of viral particles with and without the P2 protein are indistinguishable (Yan *et al.*, 1996). These facts suggest that the basic morphological organization of the outer capsid of the virus depends on the arrangement of the P8 prtotein as well as the P8 protein is related to the in fection.

II-1.3 Materials and Methods

Purification of the P8 prtoein

The O strain of RDV (Kimura *et al.*, 1987). Infected rice leaves were macerated with a meat chopper, clarified by treatment with CCl_4, and subjected to differential centrifugation in 10 to 40% and 40 to 60% sucrose. The final pellet after high-speed centrifugation of the materials in the band of viral particles was suspended in a 0.1M solution of histidine that contained 0.01M $MgCl_2$, pH6.2 (His-Mg).

High concentrations of $MgCl_2$ have been used to remove P8 protein from intact RDV particles (Takahashi *et al.*, 1994). The preparation of viral particles was adjusted to 0.8M MgCl2 in His-Mg, incubated for 5min at room temperature, and centrifuged for 10min at 200,000 × *g* at 4°C in a model TL-100 rotor (Beckman, Palo Alto, Calif.). The supernatant contained P8 and a very small amount of P3 protein.

The protein was further purified by gel filtration fast-protein liquid chromatography on column of Superdex 200 HR 10/30 (Pharmacia, Uppsala, Sweden) in 0.8M $MgCl_2$ in His-Mg. Fractions corresponding to the major peak of protein were pooled and concentrated with an Amicon diafiltration unit with a 10-kDa normal molecular mass cutoff membrane (Centricon; Amicon, Beverly, Mass). Sodium dodecyl sulfate-polyacrylamide gel electrophoresis on a 10% acrylamide gel (Laemmli, 1970) yielded a single band.

Crystallization of the P8 protein

The concentration of $MgCl_2$ in the preparation of P8 protein was varied by dialysis against different target concentrations of $MgCl_2$ at 4°C for 2 days. The resulting solutions were transferred to microtubes and stored on ice. Preparation of P8 protein occurred at concentrations of $MgCl_2$ below 0.1M.

Elecron microscopy

Samples of purified protein were dropped onto carbon-coated 400-mesh copper grids. Samples were negatively stained with 1% uranyl acetate and examined with an electron microscope (model JEM1010; JEOL, Tokyo, Japan) operated at 100 kv. Images of crystals were recorded at a magnification of 100,000.

Image processing

The image of a 2D crystal was digitized with a Leaf Scan-45 densitometer (a Scitex Company, Herzlia, Israel) and processed on a DEC/Alpha

3000/400 (Maynard). With computer programs essentially as described by Henderson et al. (Henderson *et al.*, 1990).

II-1.4 RESULTS

2D Crystal

Small 2D crystals were observed at concentrations of $MgCl_2$ below 0.1M at 4°C (Fig. 1). Moreover, when the concentration of the ion in the sample solution was reduced to 1/30 at 16°C using *MW* 12,000 cutoff membrane, longer 2D crystals were observed. The width of them showed constant value 40nm. However, they had a variable length (ranging from sub-μm to about 1 μm). In these slender 2D crystals, in addition to the flat region, a twisted region was also observed at almost same spacing (20~nm).

Noise-filtered image

The small 2D crystal formed at 4°C was chosen to produce the noise-filtered image (Fig. 2). The lattice constant of 97Å was observed at optical diffraction pattern. Figure 2 shows the filtered image. Uniform arrangements of a small-hole lattice were observed in noise-filtered images. The capsomer, the unit formation of the capsid protein, resembled an equilateral triangle with sides of approximately 6nm. Two capsomeres were included in one lattice whose constant was about 11nm. Six triangular capsomeres formed a hexagonal cavity about 2nm in diameter.

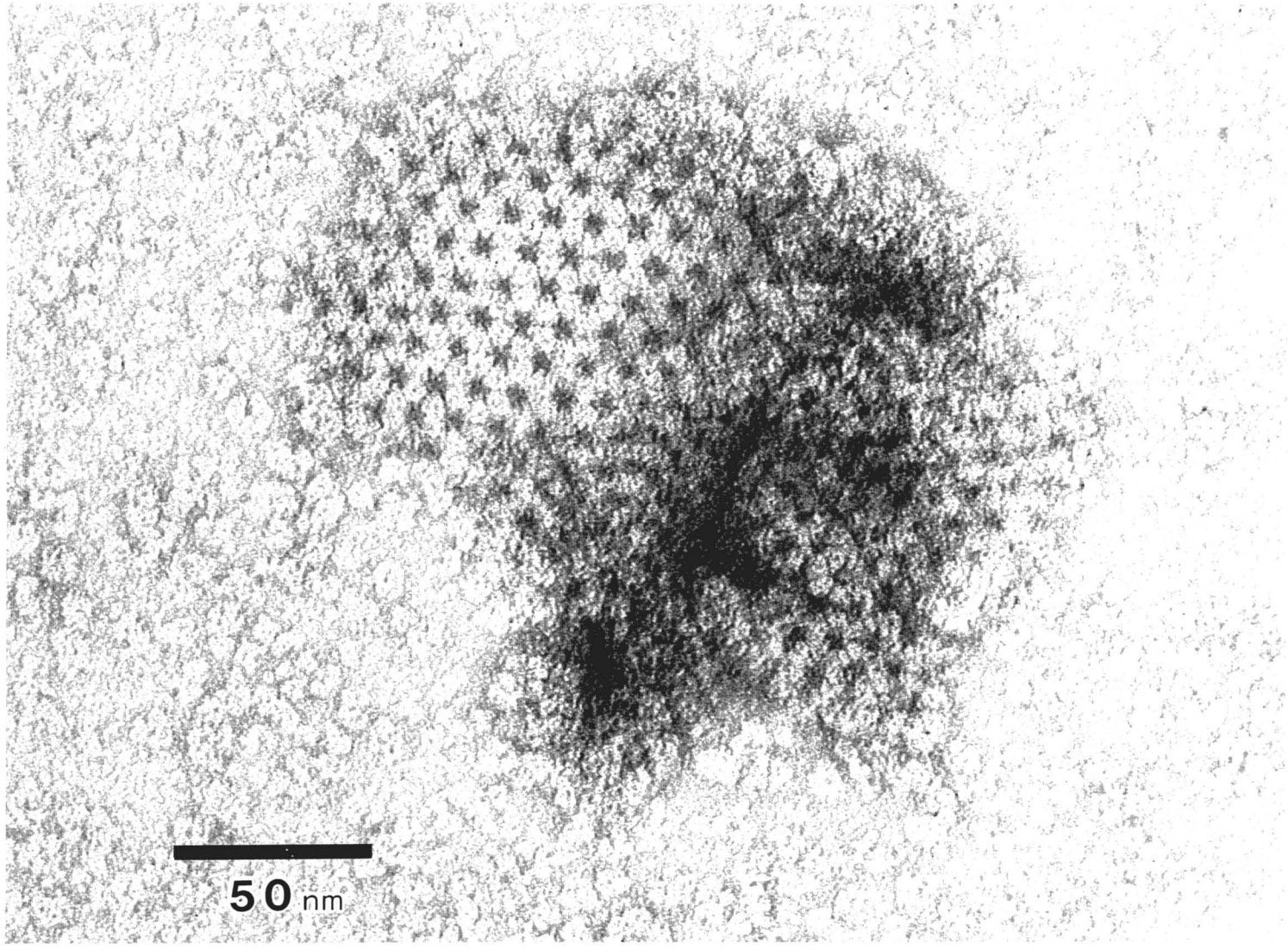

Figure 1. High magnification over view of a small 2D crystal. The triangular unit can be seen in this image of negative stained crystal.

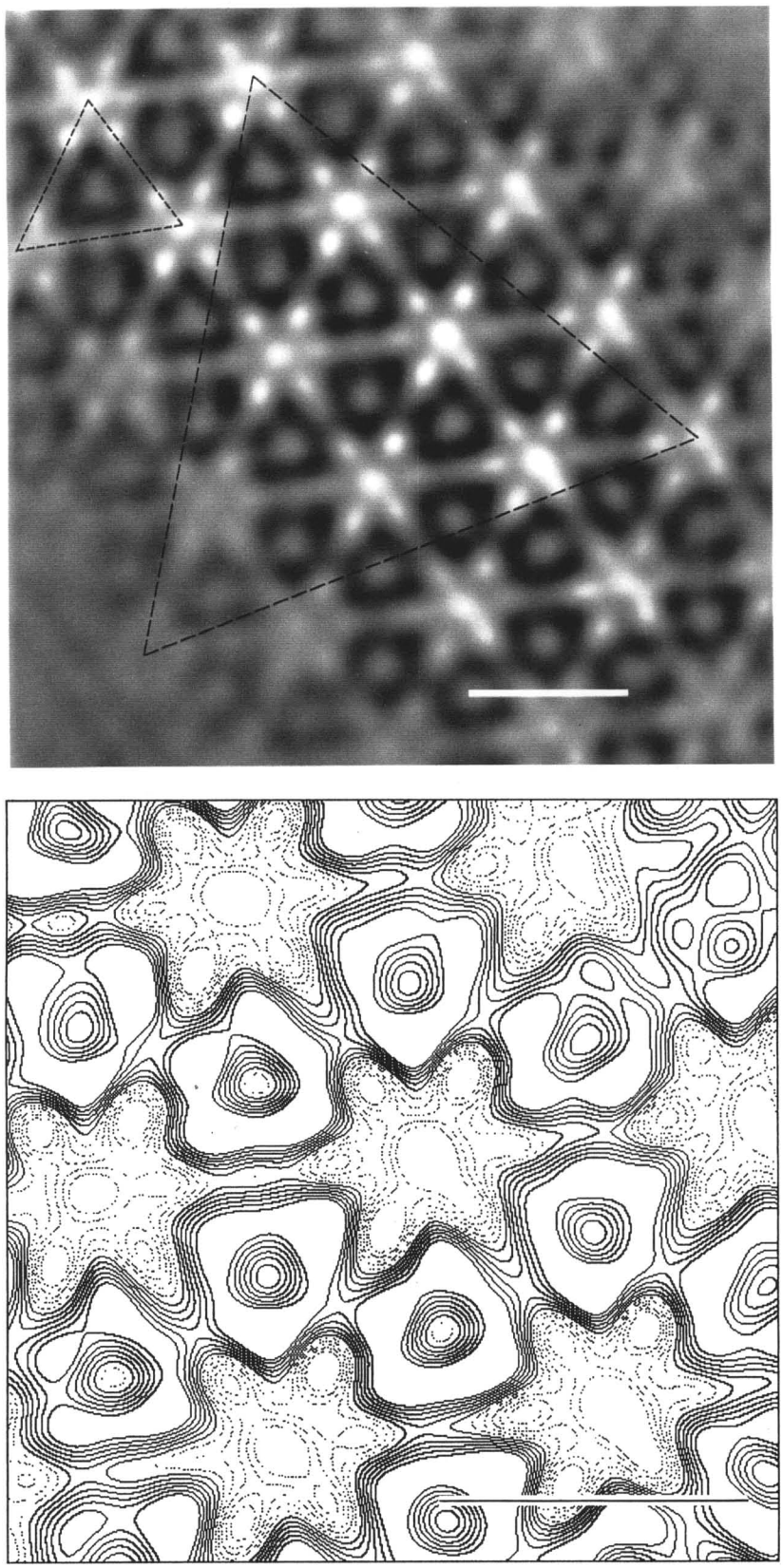

Figure 2. *a*, Fourier noise-filtered, magnified view of an array, which is displayed in gray levels, with the protein shown as black areas. A capsomere is outlined by short dashes. The area corresponding to one face of a virus particle as shown by Lu et al. *b*, is surrounded by long dashes. b, Contour map of part of the array shown in panel (a). Bars 10nm.

Trimer

To confirm that the P8 protein has the capacity to form trimers, the material used for 2D crystalization that has been dialyzed against 0.1M $MgCl_2$ was subjected to SDS-PAGE in a 10% polyacrylamide gel. A faint band of a protein with an estimated molecular mass of 140kDa, in addition to the band of P8, was detected (data not shown). This band was recognized specifically by antiserum against the P8 protein.

To characterize in further detail the futures of the P8 timer, we treated samples with 2-mercaptoethanol (2-ME) or 6M urea as described by Sabara et al (1987). Because the band of the 140-kDa protein was too weak to be recognized upon analysis of urea-treated protein that had been obtained from a peak fraction after gel filtration, purified viral particles without P2 (Yan *et al.*, 1996) were subjected to the analysis. The sample buffers contained the following components: (i) 0.0625M Tris-HCl (pH6.8), 4% SDS, and 5% 2-ME; (ii) 0.0625M Tris-HCl (pH6.8) and 4% SDS; and (iii) 0.0625M Tris-HCl (pH6.8), 4% SDS, and 6M urea. A new band of a protein of 140kDa that was not detected in the presence of 2-ME was observed in the presence of 6M urea (Fig. 3). The results were identical when samples were boiled in the same solutions for 3min at 100°C (data not shown). The 140-kDa protein reacted with the antiserum against the P8 protein on a Western blot (data not shown).

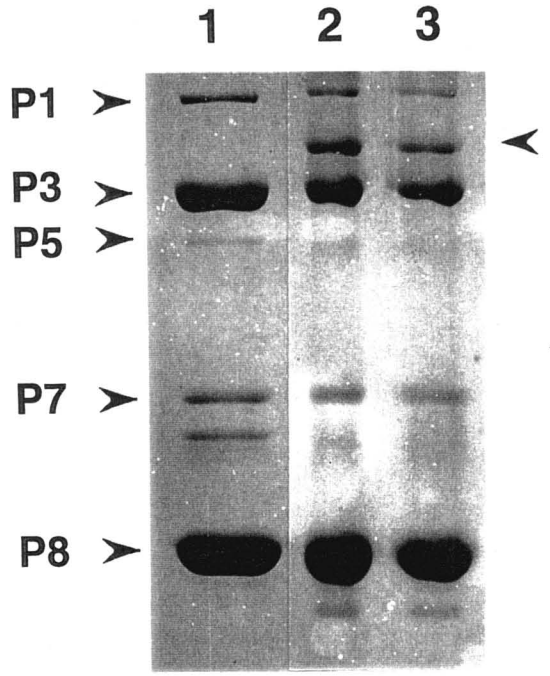

Figure 3. Protein profiles of (P2-free) RDV after SDS-PAGE (10% polyacryamide). Lane: 1, preparation of virus treated with 2-ME-containing buffer; 2, preparation of virus treated with buffer without 2-ME; 3, preparation of virus treated with urea-containing buffer. The components each buffer are given in the text. A new band is indicated by an arrowhead on the right. Positions of virus component proteins are shown on the left (refer to Fig. 2)

II-1.5 DISCUSSION

It is evident that the concentration of the ion plays an key role in the production of the 2D crystals. However, how the width and the length of the 2D crystals of P8 proteins are determined has never been resolved. One of the reasons might be that the assembly of the P8 proteins form a curve, because the P8 proteins are used to form the icosahedral virus particle. The twists also might be caused by this reason. Eventually, it is difficult to make a large 2D crystal.

The noise-filtered image shows the cavity surrounded by the six triangular subunits. These cavities might be candidates for a path by which solutes can enter and viral mRNA can leave the virus particle without any treatment (Kodama *et al.*, 1973), as has been proposed for the core particles of rotavirus (Prasad *et al.*, 1988). Because the surface lattice of the 2D crystals was similar to those observed on virus particles (Lu *et al.*, 1995; Omura *et al.*, 1989; Uyeda & Shikata, 1982). Furthermore, the 2D crystals were formed under the same conditions as those under which virus particles can be reconstructed from their core and outer capsid components (Takahashi *et al.*, 1994). These observations suggest that a local lattice of P8 in an intact RDV particle is not very different from that in our 2D crystals.

A triangular capsomere can be formed reasonably from three units. Such a model, together with calculations of volume (Omura *et al.*, 1989), indicates that the capsomere is a trimer of the P8 protein. Since the 140-kDa protein was recognized by antiserum against the P8 protein, this model was shown to be right. The fact that the 140-kDa protein was generated from material that has eluted as a single peak during gel filtration also indicated that the 140-

kDa protein originated from monomers of the P8 protein or that the P8 protein was the product of dissociation of the 140-kDa protein. In any case, it is clear that P8 has the ability to form trimers.

The band of the protein of the 140-kDa was diminished when the purified viral particles without P2 was treated with 2-ME. However, this band was observed in the presence of 6M urea. In addition to the fact that the 140-kDa protein reacted with the antiserum against the P8 protein, this result demonstrates that the unit structure of the outer capsid of RDV is composed of trimers of P8 protein linked by disulfide bonds. It is consistent with the data that RDV is composed of capsomeres, which consist of three protein subunits (Lu *et al.*, 1995).

In all viruses that belong to the family Reoviridae and have been studied to date, the second layers of the virus particles are all composed of trimers. Thus, μ1, a major outer capsid protein of reovirus (Dryden *et al.*, 1993); VP6, a major protein of the single-shelled rotavirus (Prasad & Chiu, 1994; Prasad *et al.*, 1996); and VP7 , a core surface protein of bluetongue virus (Roy, 1996), all form trimers. The packaging of the symmetrical clusters in the trimer of RDV P8 protein is distinct from that of VP6 of rotavirus, whose clusters are packaging asymmetrically when they re assembled in vitro (Bellamy & Both, 1990; Reddy *et al.*, 1992). The morphological and/or biological implications of this common structure in reoviruses that infect plants, insects, and mammals remain to be clarified.

The area surrounded by dashes in Fig. 2 correspnds to one face of a virus particle (T=13), shown in a reconstructed three-dimensional figure of RDV (Lu, 1995). P8 capsid protein by itself did not form icosahedral particles under our conditions. Therefore, it seems that the triangular clusters need

another protein to support interactions between them.

II-1.6 ACKNOWLEDGEMENTS

I am grateful to Yafeng Zhu for sending purified sample and finding the disulfide bonds between monomers of P8 proteins.

I also would like to thank Dr. Kaoru Mitsuoka for helping image analysis.

II-1.7 REFERENCES

Bellamy, A. R. & Both, G. W. (1990). Molecular biology of rotaviruses. *Adv. Virus. Res.* **38**, 1-43.

Boccardo, G., Milne, R. G., Disthaporn, S., Chettanachit, D. & Putta, M. (1985). Morphology and nucleic acid of rice gall dwarf virus. *Intervirology.* **23**, 167-171.

Dryden, K. A., Wang, G., Yeager, M., Nibert, M. L., Coombs, K. M., Furlong, D. B., Fields, B. N. & Baker, T. S. (1993). Early steps in reovirus infection are associated with dramatic changes in supramolecular structure and protein conformation: analysis of virions and subviral particles by cryoelectron-microscopy and image reconstruction. *J. Cell. Biol.* **122**, 1023-1041.

Henderson, R., Baldwin, J. M., Ceska, T. A., Zemlin, F., Beckmann, E. & Downing, K. H. (1990). Model for the structure of bacteriorhodopsin based on high-resolution electron cryomicroscopy. *J. Mol. Biol.* **213**, 899-929.

Holmes, I. H., Boccardo, G., Estes, M. K., Furuichi, M. K., Hoshino, Y., Joklik, W. K., McCrae, M., Mertens, P. P. C., Milne, R. G., Samal, K. S. K., Shikata, E., Winton, J. R., Uyeda, I. & Nuss, D. L. (1995). Family Reoviridae. *Arch. Virol. Suppl.* **10**, 208-239.

Kimura, I & Shikata, E. (1968). Structural model of rice dwarf virus. *Proc. Jpn. Academy.* **44**, 538-543

Kimura, I., Minobe, Y. & Omura, T. (1987). Changes in a nucleic acid and a protein component of rice dwarf virus particles associated with an increase in symptom severity. *J. Gen. Virol.* **68**, 3211-3215.

Kodama, T. & Suzuki, N. (1973). RNA polymerase activity in purified rice dwarf virus. *Ann. Phytopathol. Soc. Jpn.* **39**, 251-258.

Laemmli, U. K. (1970). Cleavage of structural proteins during the assembly of the head of bacteriophage T4. *Nature.* **277**, 680-685.

Lu, G., Zhou, Z. H., Jakana, J., Deyou, C., Shengxiang, C., Xincheng, W., Xiaocheng, G. & Chiu, W. (1995). Three-dimensonal structure of rice dwarf virus by electron cryomicroscopy. *High Technology Letters.* **1**, 1-4

Nakata, M., Fukunaga, K. & Suzuki, N. (1978). *Polypeptide components of rice dwarf virus. Annals of the Phytopathological Society of Japan.* **44**, 288-296

Noda, H., Ishikawa, K., Hibino, H., Kato, H. & Omura, T. (1991). Nucleotide sequences of genome segment S8, encoding a capsid protein, and S10, encoding a 36K protein, of rice gall dwarf virus. *J. Gen. Virol.* **72**, 2837-2842

Omura, T. & Inoue, H. (1985) Rice gall dwarf virus. *CMI/AAB Descriptions of Plant Viruses* No. 296

Omura, T., Ishikawa, K., Hirano, H., Ugaki, M., Minobe, Y., Tsuchizaki, T. & Kato, T. (1989). The outer capsid protein of rice dwarf virus is encoded by genome segment S8. *J. Gen. Virol.* **70**, 2759-2764

Omura, T., Minobe, Y., Matsuoka, M., Nozu, Y., Tsuchizaki, T. & Saito, Y. (1985). Location of structural proteins in particles of rice gall dwarf virus. *J. Gen. Virol.* **66**, 811-815.

Plasad, B. V. V. & Chiu, W. (1994). Structure of rotavirus. *Curr. Top. Microbiol. Immunol.* **185**, 9-29.

Plasad, B. V. V., Rothnagel, R., Zeng, C. Q.-Y., Jakana, J., Lawton, J. A., Chiu, W. & Estes, M. K. (1996). Visualization of urdedd genomic RNA and localization of transcriptional complexes in rotavirus. *Nature.* **382**, 471-473.

Reddy, D. V. R. & Macleod, R. (1976). Polypeptide components of wound tumor virus. *Virology.* **70**, 274-282.

Prasad, B. V. V., Wang, G. J., Clerx, J. P. M & Chiu, W. (1988). Three-dimensional structure of rotavirus. *J. Mol. Biol.* **199**, 269-275.

Reddy, D. A., Bergmann, C. C., Meyer, J. C., Berriman, J., Both, G. W., Coupar, B. E. H., Boyle, D. B., Andrew, M. E. & Bellamy, A. R. (1992). Rotavirus VP6 modified for expression on the plasma membrane forms arrays and exhibits enhanced immunogenicity. *Virology.* **189**, 432-434.

Roy, P. (1996). Orbivirus structure and assembly. *Virology.* **216**, 1-11.

Sabara, M., Ready, K. F. M., Frenchick, P. J. & Babiuk, L. A. (1987). Biochemical evidence for the oligomeric arrangement of bovine rotavirus nucleocapsid protein and its possible significance in the immunogenicity of this protein. *J. Gen. Virol.* **68**, 123-133.

Streissle, G. & Granados, R. R. (1968). *The fine structure of wound tumor virus and reovirus. Archiv Gesamte Virusforschung.* **25**, 369-372.

Suzuki, N. (1995). Molecular analysis of the rice dwarf virus genome. *Semin. Virol.* **6**, 89-95.

Takahashi, Y., Tomiyama, M., Hibino, H. & Omura, T. (1994). Conserved primary structures in core capsid proteins and reassembly of core particles and outer capsids between rice gall dwarf and rice dwarf phytoreoviruses. *J. Gen. Virol.* **75**, 269-275.

Uyeda, I. & Shikata, E. (1982). Ultrastructure of rice dwarf virus. *Ann. Phytopath. Soc. Jpn.* **48**, 295-300

Xu, Z., Anzola, J. V. & Nuss, D. L. (1989). Assignment of wound tumor virus nonstructural polypeptides to cognate dsRNA genome segments by in vitro expression of tailored full-length cDNA clones. *Virology.* **168**, 73-78.

Yan, J., Tomaru, M., Takahashi, A., Kimura, I., Hibino, H. & Omura, T. (1996). P2 protein encoded by genome segment S2 of rice dwarf phytoreovirus is essential for virus infection. *Virology.* **224**, 539-541.

CHAPTER II-2

Herical reconstruction of the tubular crystal of P8 capsid protein

II-2.1 SUMMARY

Tubular crystals were obtained from purified P8, an outer capsid protein of rice dwarf phytoreovirus, and the structure was determined by electron cryomicroscopy at 9Å. Moreover, in this chapter, I report a multi-domain structure of P8 protein in the trimer units that form the tubular crystal.

Tubular crystals were obtained by dialysis of the sample solution against distilled water. The tubular crystal embedded in vitreous ice was examined by an electron microscope with a liquid-helium stage and a field emmision electron gun. From 11 good images, a three-dimensional image was reconstructed using helical image analysis. The tube consists of a pair of trimers of P8 proteins. The two trimer axis are slight twisted from the parallel arrangement. The pairing results in crystallographic two fold symmetry of the tube and the trimer are related by non-crystallographic symmetry. These symmetries were used to refine the structure factors. The pyramid-like monomer structure was revealed to contain five domains. The fin-like domain faces the outer surface of the tube, which is presumably related to the infectious function of the virus. The bottom domain of the pylamid forms the

interaction between the trimers. The middle domain connects these two domains. Two Rod-like domains are at the trimer-trimer interface.

II-2.2 INTRODUCTION

As described in Chapter II-1, rice dwarf virus (RDV) is a phytoreovirus that is a member of the family *Reoviridae* (Holmes *et al.*, 1995). This virus structure is divided into three parts: (1) an outer shell diameter with a 693Å (Mizuno *et al.*, 1991; Uyeda & Shikata, 1982), (2) a core particle inside the outer shell, (3)12 segments of double-stranded RNA and four species of proteins inside the core particle. The outer shell of RDV is composed of 260 capsomeres (Lu *et al.*, 1995), and the molecular mass of the capsomere, 138.5 kDa, suggests that a capsomere is composed of three molecules of P8 proteins (Omura *et al.*, 1989). The outer capsid layer is also composed of minor P2 besides major P8 proteins (Yan *et al.*, 1996). While the P2 protein was recently shown to be esential for infection (Yan *et al.*, 1996), the P8 protein appears to be also involved in infection because neutralizing antibodies can be raised against this protein (Omura, Unpublished). The appearances of viral particles with and without the P2 protein are indistinguishable (Yan *et al.*, 1996). These facts suggest that the basic morphological organization of the outer capsid of the virus depends on the arrangement of the P8 proteins.

II-2.3 Materials and Methods

Tubular crystls preparation

The P8 protein was purified from the intact RDV as described in Chapter II-2 (Zhu *et al.*, 1997). The P8 protein in 0.1 M histidine-Mg buffer (pH 6.2) containing 0.8 M $MgCl_2$. This solution was dialyzed against various kinds of buffer solutions, using Slide-A-Lyzer 10k Dialysis Cassettes (PIERCE, Rockford, Illinois, U.S.A) or dialysis cups (Daiichikagaku, Tokyo, Japan) with a 3,500-Da normal molecular mass cutoff membrane, at 16 °C. The solutions containing the P8 proteins were transferred to the microtubes and stored at 4°C. Tubular crystals of P8 were grown in 2~3 days. After the tubular crystals were formed, the solutions were treated carefully because the tubular crystals tend to be broken by mechanical purturbation, such as pipetting or centrifugation.

Electron microscopy

Portion (2.5 μm) of solutions containing the tubes were applied to the carbon side of holey carbon supported grids, which were glow dischared. Excess solution was blotted off and the grids were plunged into liquid ethane slush to embed the specimens in amorphous ice. Specimens were examined at low temperatures between 4 K and 20 K, using JEM-3000SFF (JEOL, Tokyo, Japan) operating at 300 kV. Electron micrographs were recorded on Kodak SO-163 with a low dose kit, at magnification of 40,000x and 2s exposure time. The electron dose estimated from the current density was 17

to 20 electrons/Å^2. The films were developed for 14min in D19 developer.

Rotary-shadowing

The tubular crystals embedded in vitreous ice were transferred to a JEE-4X rotary evaporator (JEOL), the inside of which was evaporated. Then, the specimens were rotary shadowed at an elevation angle of 7.5° with platinum/carbon and backed by carbon using a JEE-400 vacuum evaporator (JEOL). The specimens were examined by a JEOL1010 microscope operating at 100 kV.

Image analysis

Micrographs were checked by optical diffraction to see whether helical symmetry was maintained and the notable drift was absent. Selected micrographs were digitized by a Leaf Scan-45 densitometer (Scitex Company, Herzlia, Islael), at a scanning interval of 5 μm, which corresponds to 1.25 Å on the specimen. Then, images that gave sharp and symmetrical layer-lines in computed Fourier transforms were selected.

Helical image analysis was done by the method of Toyoshima & Unwin (1988, 1990) with further improvements in the averaging procedure (Yonekura & Toyoshima, unpublished; Mimori *et al.*, 1995). A brief description of the image analysis is as follows. The Fourier transform of images of the tubular crystals shows a series of layer-lines, whose phase differences between near- and far-side should be 0° or 180° because of the

two-fold symmetry unless the tubes are not tilted largely away from the plane normal to the electron beam. Images were rejected if they gave layer-lines that were not symmetrical about the Z axis or showed large deviations in the phase differences from 0° or 180°. The helical symmetry was determined from the first peak positions of the layer lines and the phase differences between near and far side. The layer line structure factors were extracted from the Fourier transform on the layer line positions determined by the helical symmetry. The data quality of each image was evaluated from the phases after adjusting the phase origin to the 2-fold axis perpendicular to the tube axis. The structure factors are modulated by the CTF. Firstly, the phase of each image was corrected for the CTF. After averaging each image, each layer line was trimmed off for portions showing large phase differences and low figures of merit. The amplitudes of these merged and edited data were divided by the averaged ctf. Finally, after removing the effect of the amplitude modulation by the CTF, the phases were enforced to be 0° or 180°.

NCS averaging

A trimer unit was cut out from the map of the tube. After the three-fold axis was searched, the map was averaged using that axis (see Appendix).

II-2.4 RESULTS

Tubular crystal preparation

P8 in Histidine-$MgCl_2$ buffer containing 0.8 M $MgCl_2$ (pH 6.2) tends to aggregate and forms small two dimensional crystals when the concentration of 0.8M $MgCl_2$ is reduced to 0.1 M (Chapter II-1; Zhu *et al.*, 1997). When the sample solution was dialyzed against distilled water to 30 times dilution, only twisted ribbon-like 2D crystals (~40 × 400nm) were observed as described chapter II-1. However, tubular crystals appeared after dilution of the solution to 1/1750 or below. Electron micrographs of the tubular crystals showed a variable length from sub-μm to ~4 μm but a constant diameter of ~55 nm (Fig. 1a). Other conditions examined are listed in Table1. To see whether the tubular crystallization is the result of low Mg^{2+} concentration, the sample solution was dialyzed against 0.1 M histidine-$MgCl_2$ solution (pH 6.2) but only the twisted ribbons were observed. The effect of the buffer type was also examined, using five kinds of buffer with pH 6.2. The crystals were observed only in the MES buffer. When slightly different pHs (5.7 and 6.7) of the 100 mM MES-NaOH buffers were used, there were many tubular crystals formed at pH 5.7, whereas, few were observed at pH 6.7. When 1 mM NaCl or 10 mM NaCl was added to this buffer solutions, tubular crystals were found at both pHs. When many spherical particles with a diameter of ~70nm, which is almost the same size as the intact virus particle were formed at pH6.2,

Table 1

The conditions required for crystallization of tubes

Conditions	Results
1/30 dilution against distiled water	Slender 2D crystals, ~40×400nm
1/1750 dilution against distiled water	Tubes*
0.1 M Histidine-HCl, pH 6.2	Slender 2Dcrystals with twists
0.1 M Histidine-0.01M MgCl2, pH6.2	No crystals
50 mM Bis-Tris-HCl, pH 6.2	Slender 2D crystals, ~50 ×100nm
100 mM MES-NaOH, pH 6.2	Tubes*
100 mM PIPES-NaOH, pH 6.2	No crystals
100 mM ADA-NaOH, pH 6.2	No crystals
100 mM ACES-NaOH, pH 6.2	rolled 2D crystals
100 mM MES-NaOH, pH 5.7	Tubes*
100 mM MES-NaOH, pH 6.7	Tubes*
1 mM NaCl, 100 mM MES-NaOH, pH 5.7	Tubes*
10 mM NaCl, 100 mM MES-NaOH, pH 5.7	Tubes*
100 mM NaCl, 100 mM MES-NaOH, pH 5.7	No crystals

* The length of the tubes was usually from sub-μm to 4 μm~.

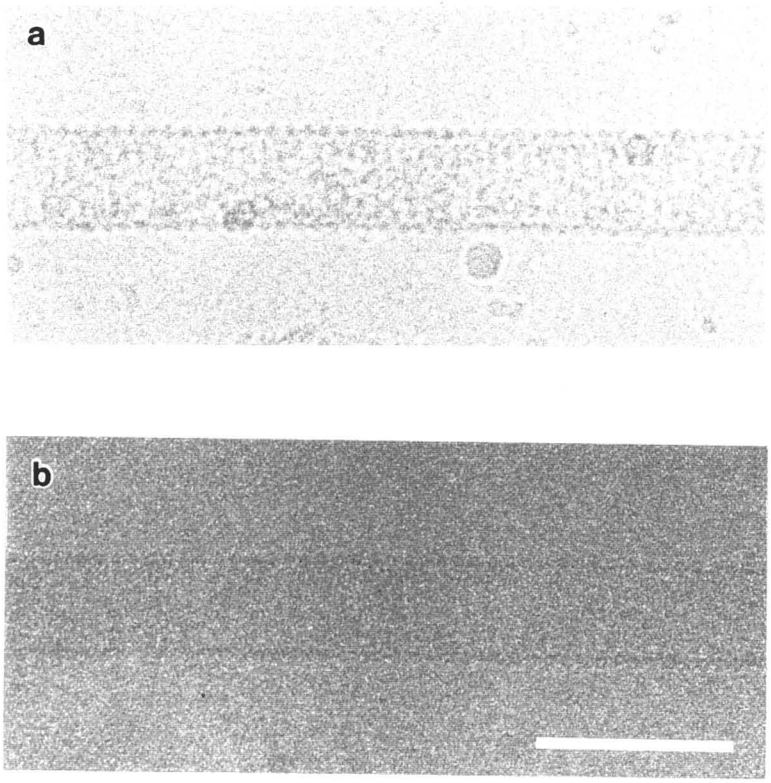
a
b

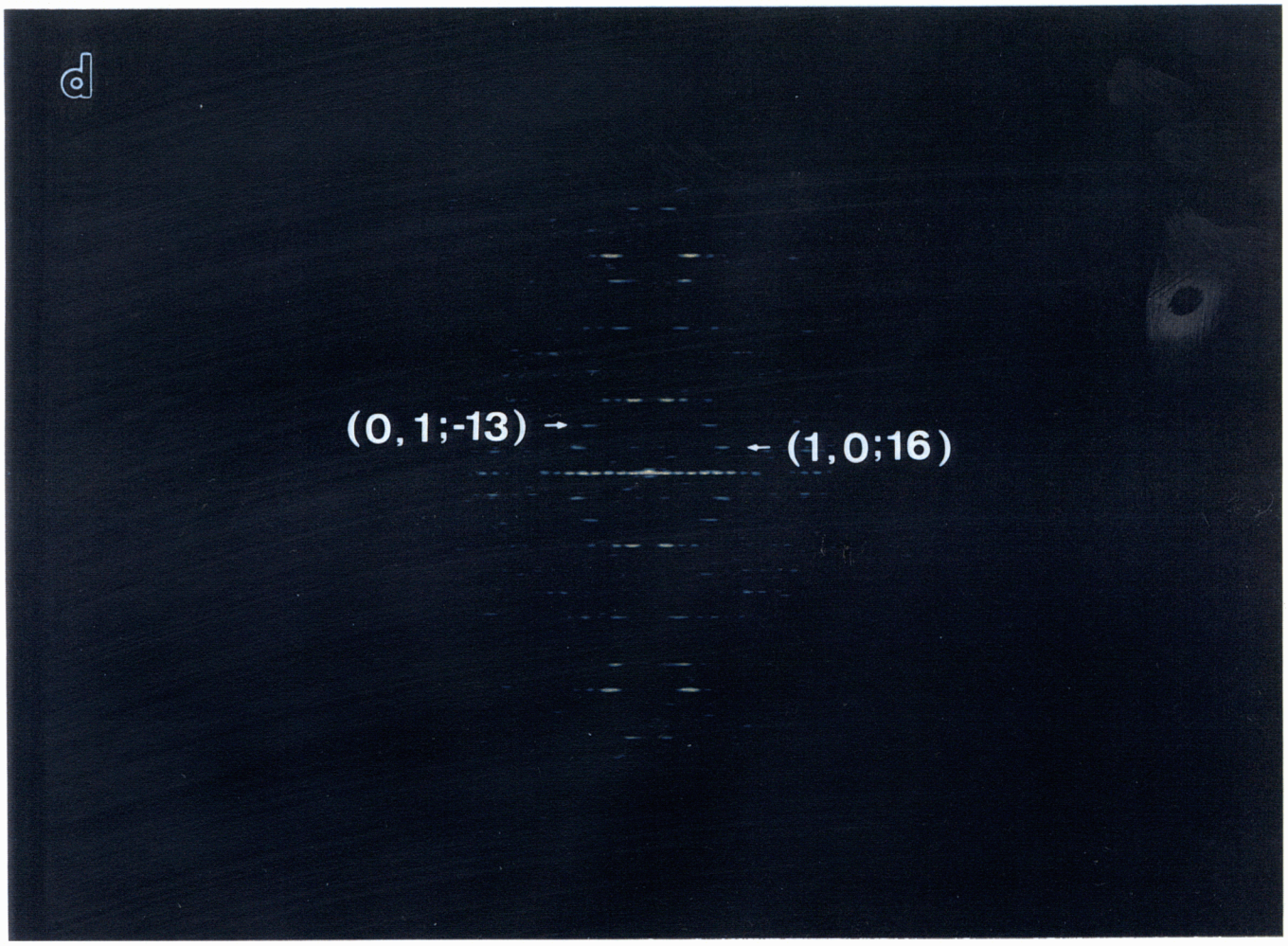

Figure 1. Images of tubes at two levels of underfocus. Defocus is 6μm (a) and 1.6μm (b). The characteristic moiré pattern was observed on (a). *c*, Rotary-shadowed replica of a tubular crystal. *d*, Computed diffraction pattern of the image of (b). Some layer lines are labeled by (h,k) indices and start numbers (Toyoshima, 1990). Bar, 100nm.

but only a small number of tubular crystals were formed. The tubular crystals were most stably formed in 100 mM MES-NaOH buffer. However, electron cryomicrographs of tubular crystals prepared in this solution showed the tubes adhered each other. Therefore, after tubular crystals were formed, the sample solution was dialyzed against distilled water.

Image of the tubular crystal

Figure 1a shows a characteristic moiré pattern observed in the cryoimage of the tube recorded at a large defocus. Images used for analysis were more weakly defocused (Fig. 1b). When the images were examined by optical diffraction, the length of the straight portion was usually < 0.5 μm. The rotary-shadowed tubes clearly showed a left-handed helical array of the subunits on the tube surface. (Fig. 1c).

Helical image reconstruction

The helical symmetry of each image was determined from the Fourier transform of the image (Figure 1d, Table 2). The radial density distribution of each tube was also obtained (Fig. 2). 11 tubes had a very similar mean radius (254±0 Å) and theoretical symmetries fell in the same helical family. These 11 tubes were used to obtain the combined data-set. Although the helical repeat distance of these tubes varied slightly, the unit cells of the selected images were very similar to each other (Fig. 3). Therefore, it was possible to combine data sets in reciprocal space, by renumbering the layer

Table 2

Profile of individual tubes

Film no.	Selection rule	Repeat distance (Å)
6900151	l=-93n+299m	1783
690020	l=-93n+299m	1765
690021	l=-107n+344m	2057
690024	l=-93n+299m	1751
690026	l=-93n+299m	1798
690043	l=-93n+299m	1790
730246	l=-93n+299m	1771
7302473	l=-200n+643m	3830
7302481	l=-93n+299m	1800
7302492	l=-144n+463m	2722

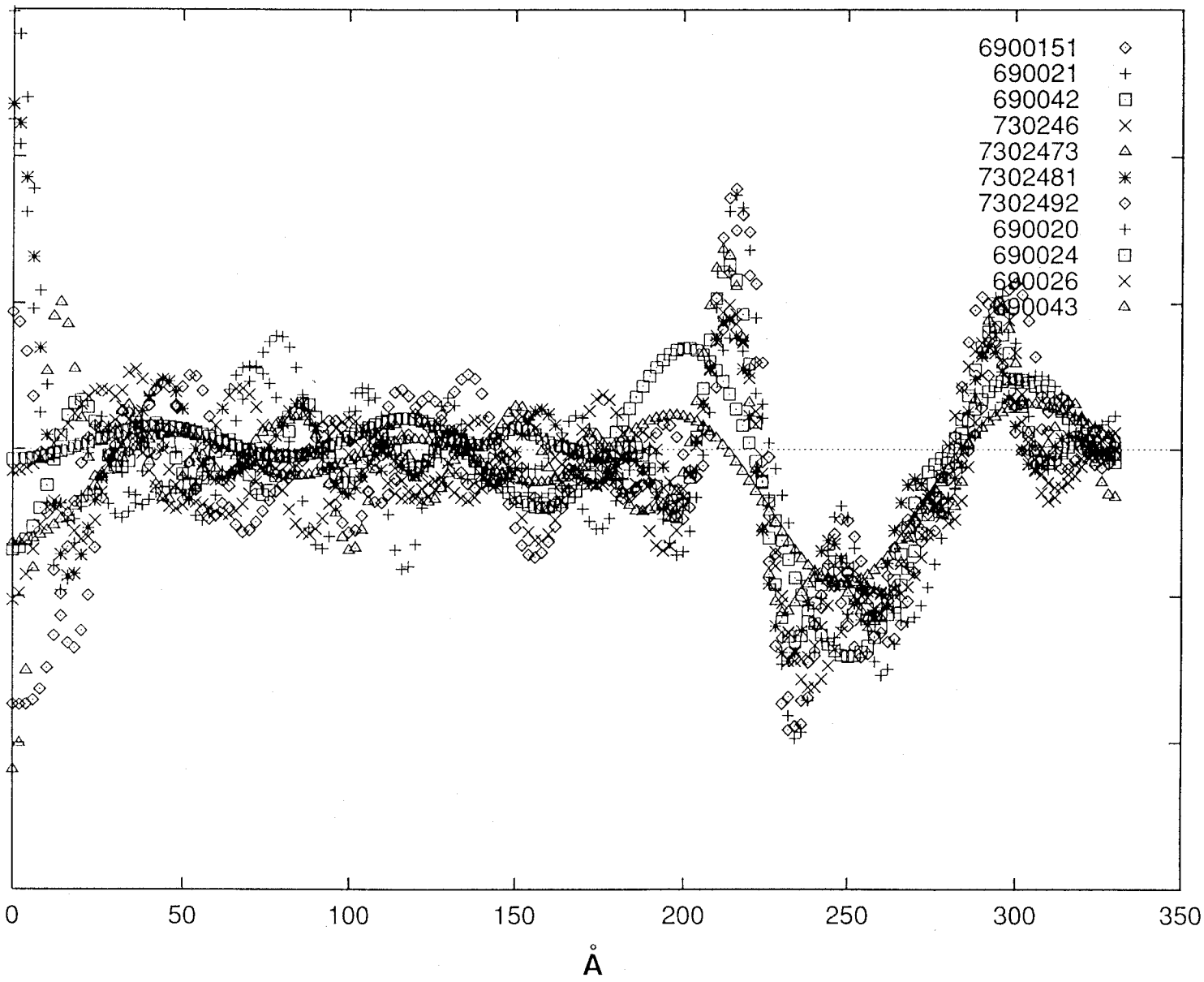

Figure 2. Mean radial density distributions of the 11 tubes. The distribution was given by a Fourier-Bessel inversion of the equatorial layer line.

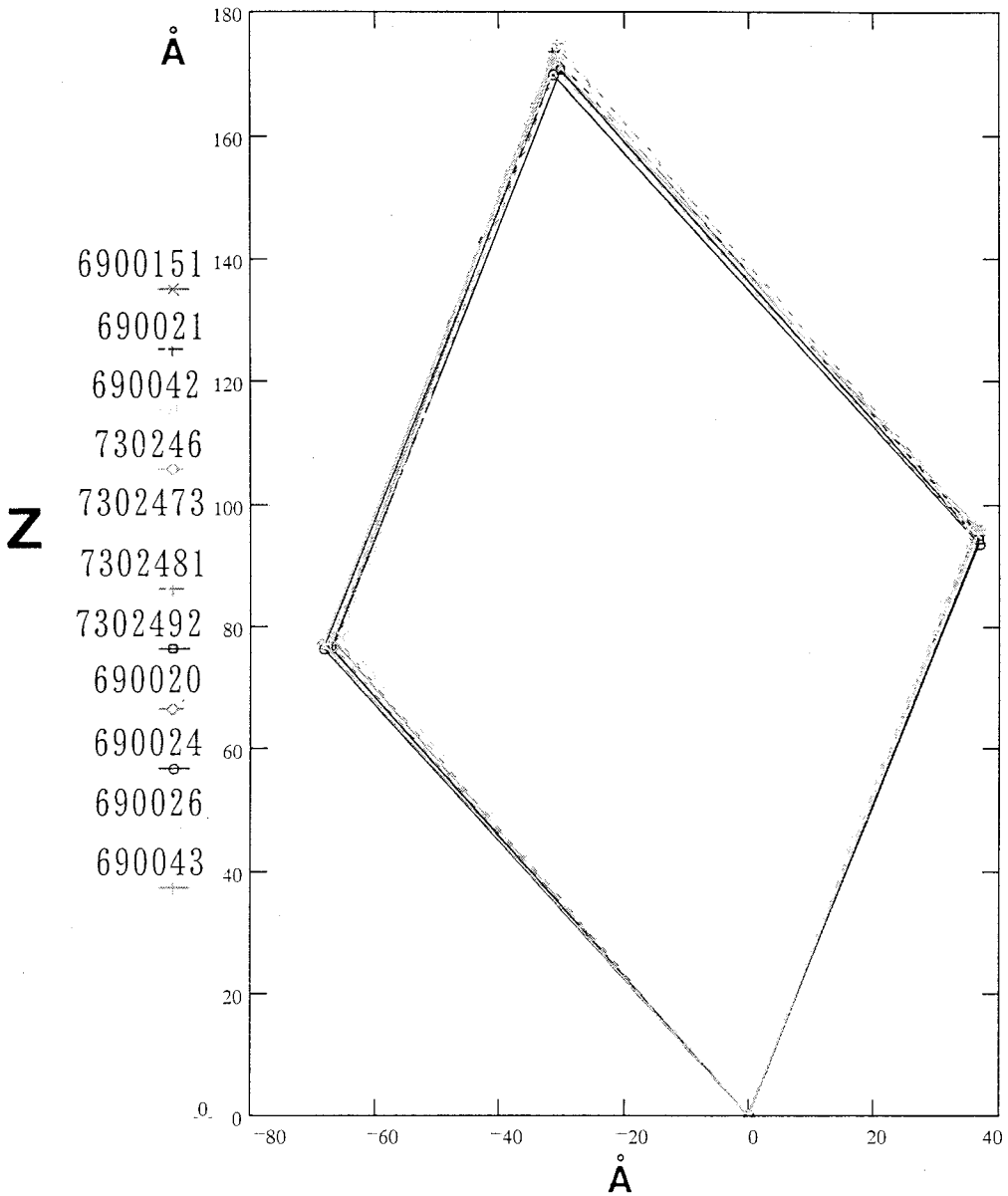

Figure 3. Unit cells of the 11tubes. Vertical axis corresponding to the longitudinal axis of tubular crystals (Toyoshima, 1990).

line orders according to those of one representative tube, without introducing significant errors. Eventually, the averaged Fourier transform yielded an amplitude-weighted 2-fold phase residual of 28° out to 7 Å resolution (Table 3).

Three-dimensional map

Figure 4 shows a surface representation of the tube, calculated from the combined Fourier terms. The outer radius of the tube is 577 Å and the inner radius is 436 Å. The triangular units corresponding to the capsomer of the virion are arranged similarly to the lattice of the small 2D crystal as previously described (Chapter I; Zhu *et al.*, 1997) . Moreover, the local subunit packing in the tube is also similar to that of the intact RDV particle. However, triangular units side by side twist each other. A pair of triangular units make the unit cell just like a lozenge. These two units rotate slightly around one of the diagonal axis of the lozenge. Six triangular subunits form hexagonal structure , at the center of which there is a hole of about 22 Å in diameter.

Three bumps around the central depression are observed on each triangular unit. The inner surface of the tube is less bumpier than the outside.

Trimer of P8

The triangular unit was cut out from the density map of the tube (Fig. 5).

Since the triangular unit of the tube corresponds to the triangular unit of the 2D crystal as described in chapter II-1, evidently, one unit is a trimer

Table 3
Phase residuals of the averaged images

resolution range (Å) Two-fold	phase residuals[1] (degree)	Completeness[2] (%)
∞-20	9	86
20-19	27	27
19-18	30	67
18-17	35	69
17-16	40	67
16-15	36	63
15-14	33	62
14-13	33	59
13-12	41	64
12-11	37	63
11-10	38	60
10-9	41	52
9-8	39	45
8-7	39	34
-7	28	49

1 Amplitude-weighted phase residuals after two-fold symmetry averaging calculated from all the Fourier terms (difference from 0° or 180°). The amplitude lower than .20% of the highest off-equatorial amplitude was cut-off.
2 The ratio of the edited data to the row data.

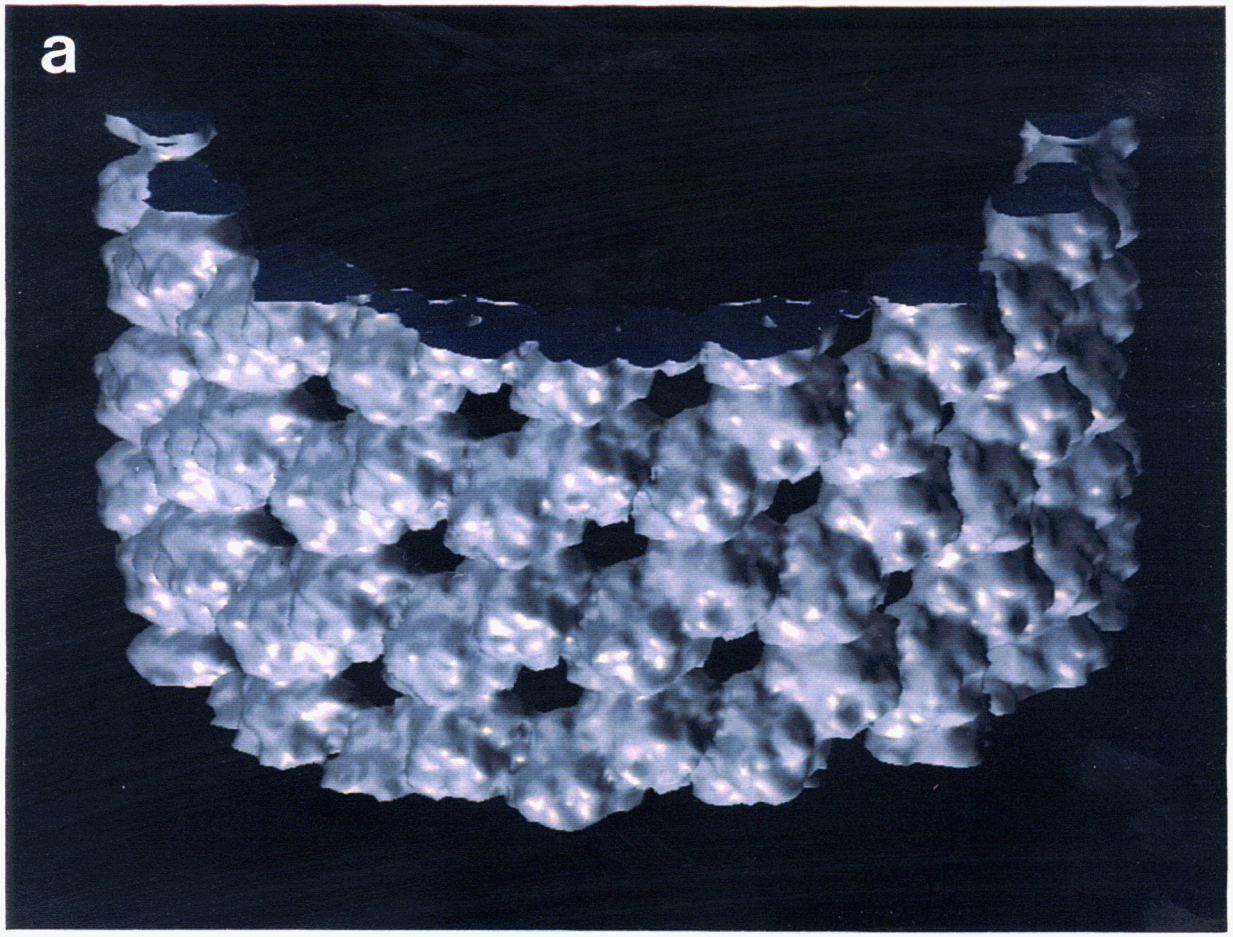
a

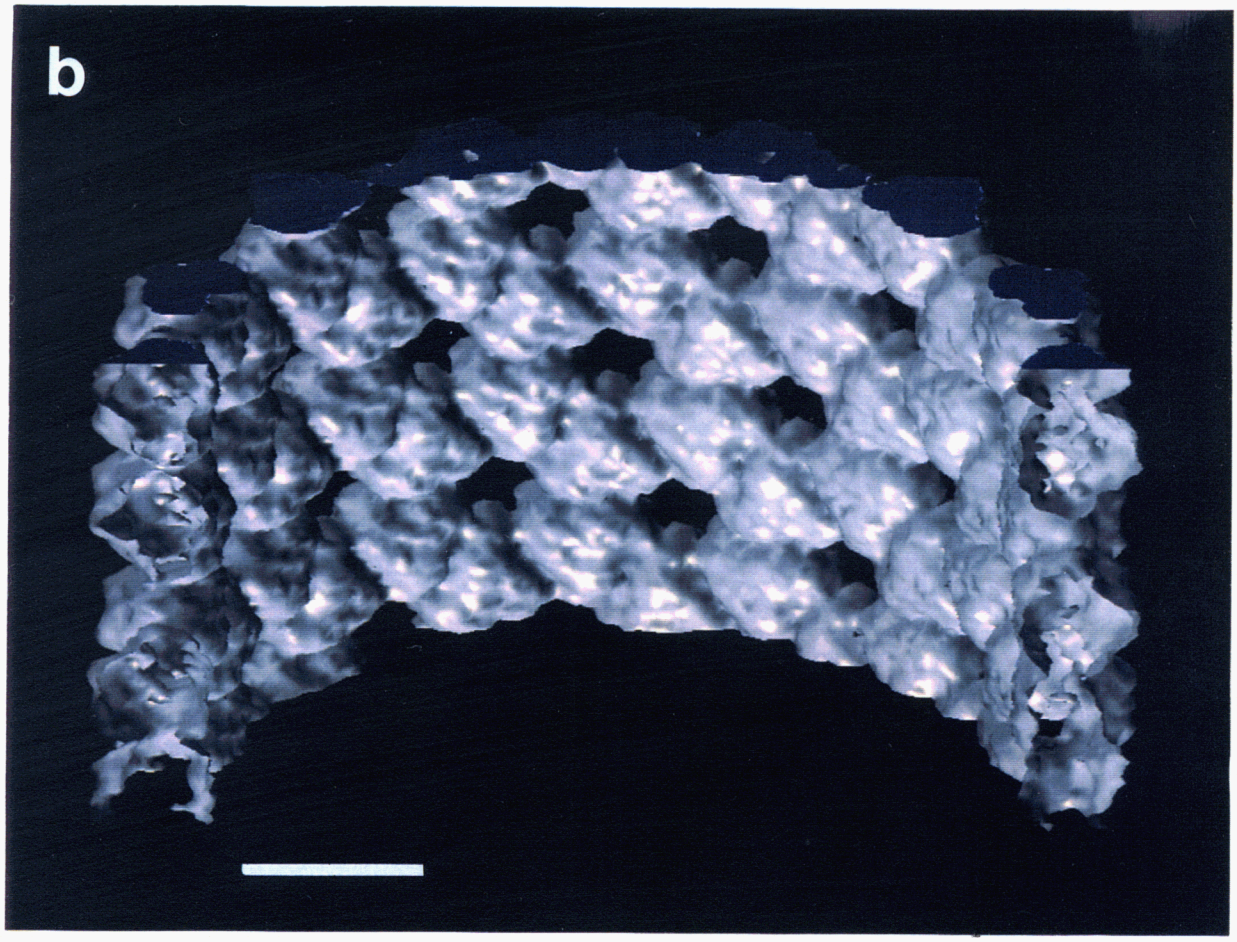
b

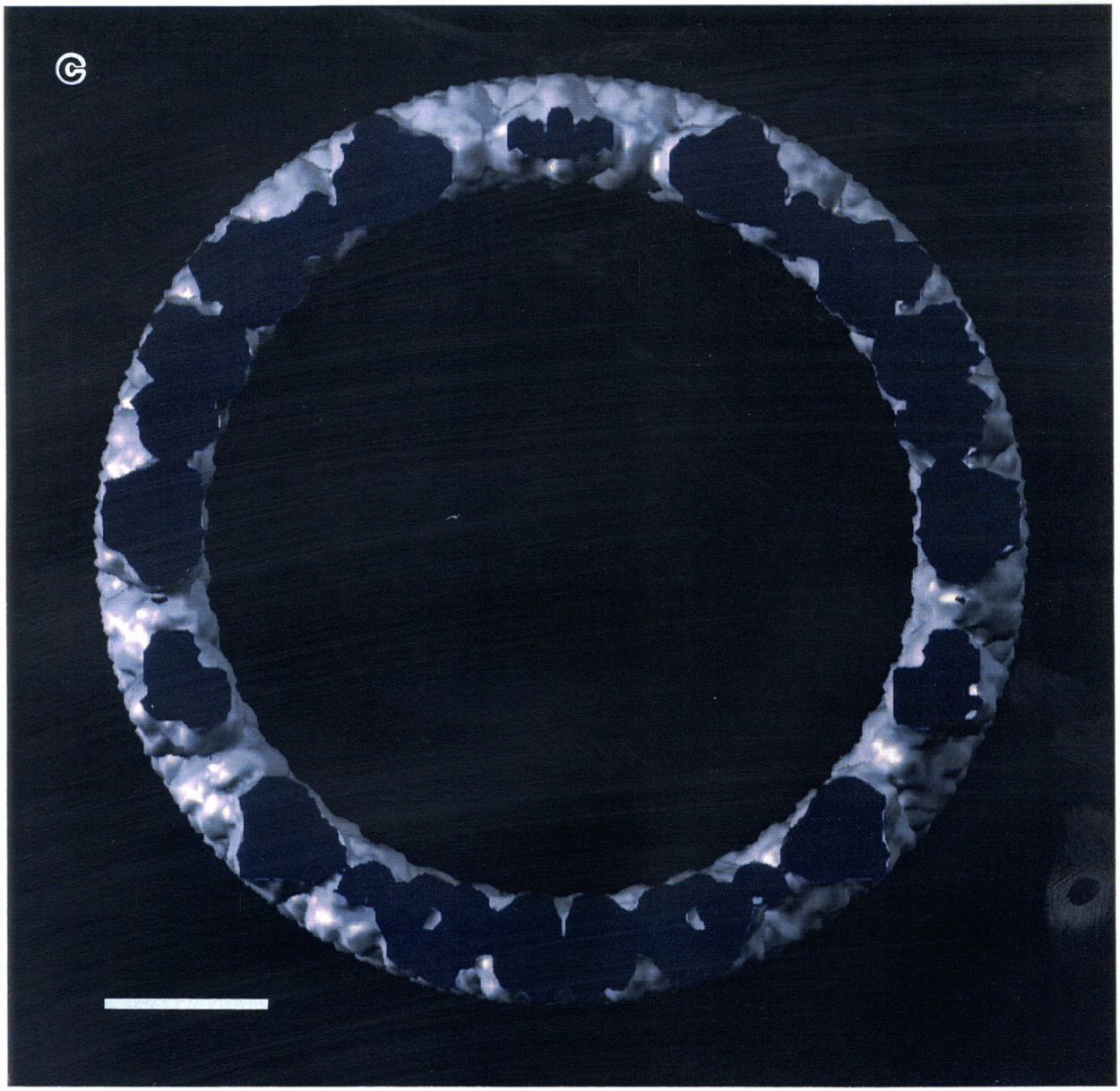

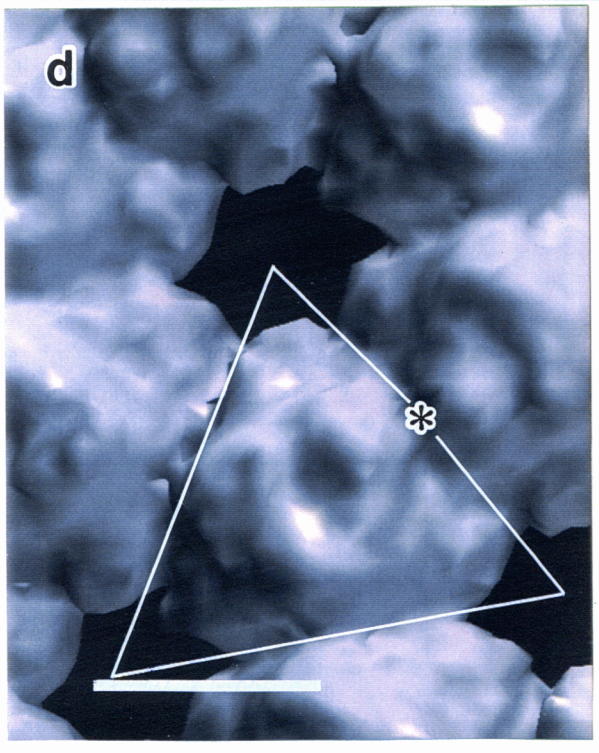

Figure 4. Three-dimensional structure of the tube. Assuming the specific volume is 1.37g/cm3, the density cutoff level for the surface models was chosen to include ~75% of the expected volume. Surface representation of the outer (a) and the inner (b) sides of the half tube cut out from the intact tube. c, Cross-section normal to the tube axis. d, Close-up of the outer sides of the tube. A star mark indicate the position of the two-fold axis; The solid flame indicates the triangular subunit corresponding to a capsomer of P8. The resolution of the maps is 9Å. Bars, 100Å in (b), (c), and 50Å in (d).

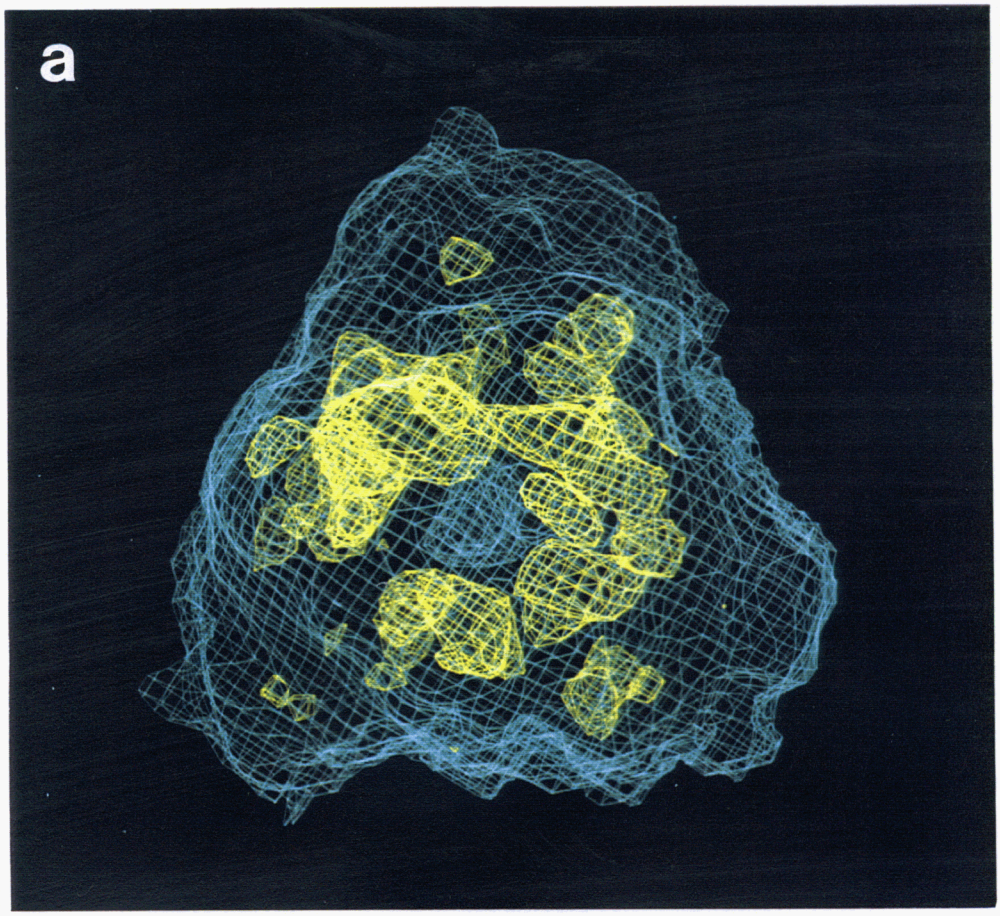
a

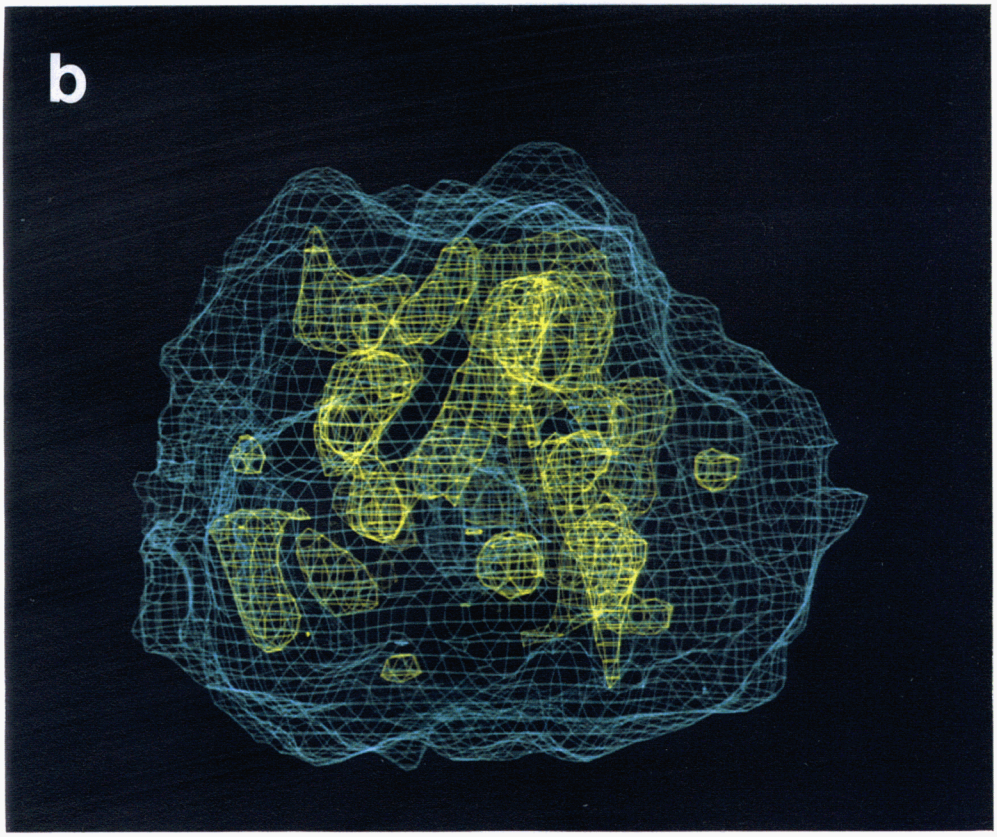
b

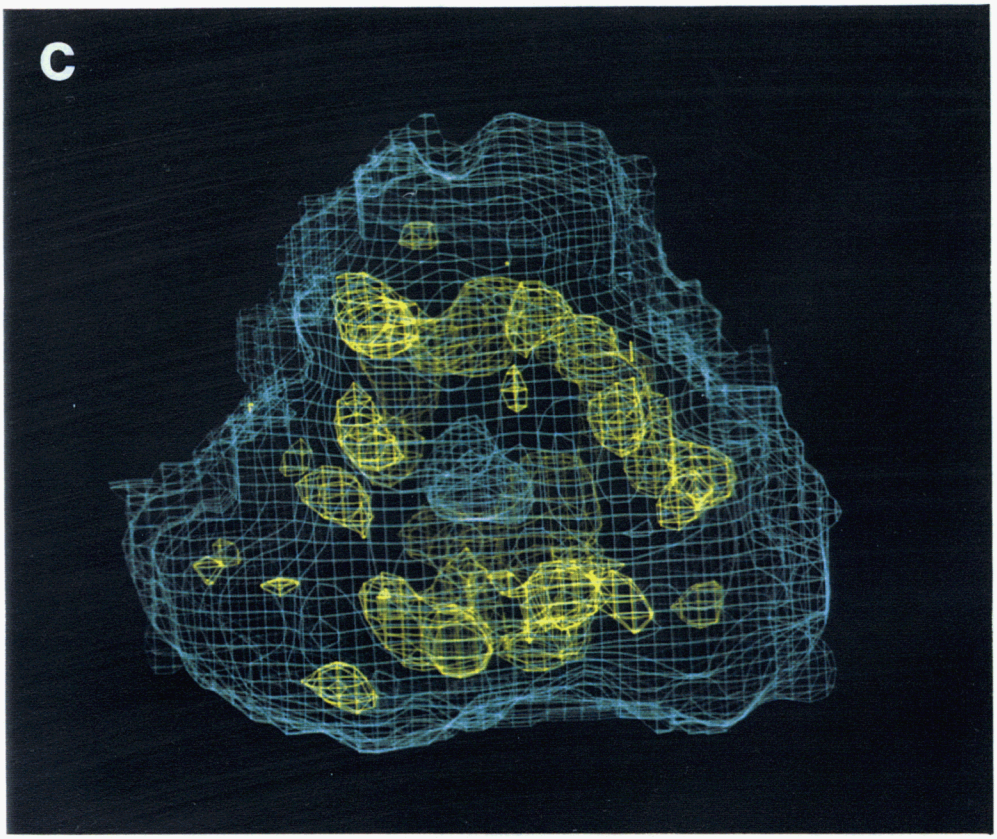

Figure 5. Fish-mesh representation of a triangular unit cut out from the density map of the tube. Green and yellow nets corresponds to 2σ and 3.8σ, respectively. *a*, view from the outer side of the tube. *b*, view approximately along the helix axis of tubular crystals. *c*, view from the inner side of the tube. The mesh size, 2Å.

of the P8 protein. Therefore, it is likely that the P8 proteins in the trimer are arranged in 3-fold positions. When the self-rotational axis of the triangular unit was examined using *almn* of the program *CCP4*, high correlation coefficients were observed at approximately 120° and 240°. Figure 6 shows 3-fold NCS-averaged structure. The triangular unit looks like a triangular pyramid, the top of which is depressed. The bottom of the pyramid forms the inner surface of the tube, and the top protrudes on the outside of the tube. The unit could be divided into three parts. At the top part, which is the outer region of the trimer, three thick fin-like domains (F). These domains appear to be packed tightly through the connector domain (C), and form low density region at the center. The middle domain is composed of two parts, one of which is a small globular domain (SG) near the end of the fin-like domain and the other part having a small rod-like domain (SR) binds to the bottom of the fin-like domain. One rod-like domain (R) and a double rod-like domain (DR) make up the bottom domain. The R domain connects to the SR domain. The rod portion of SR domain and the R domain tilts ~30° from the 3-fold axis. The tip of the SR domain is near the DR domain.

II-2.5 DISCUSSION

The mean diameter of the tube (508 Å) is smaller than that of the intact RDV particle. The tubular crystal is composed of triangular units, a pair of which occupies the unit cell. The units of the pair are related by a two-fold

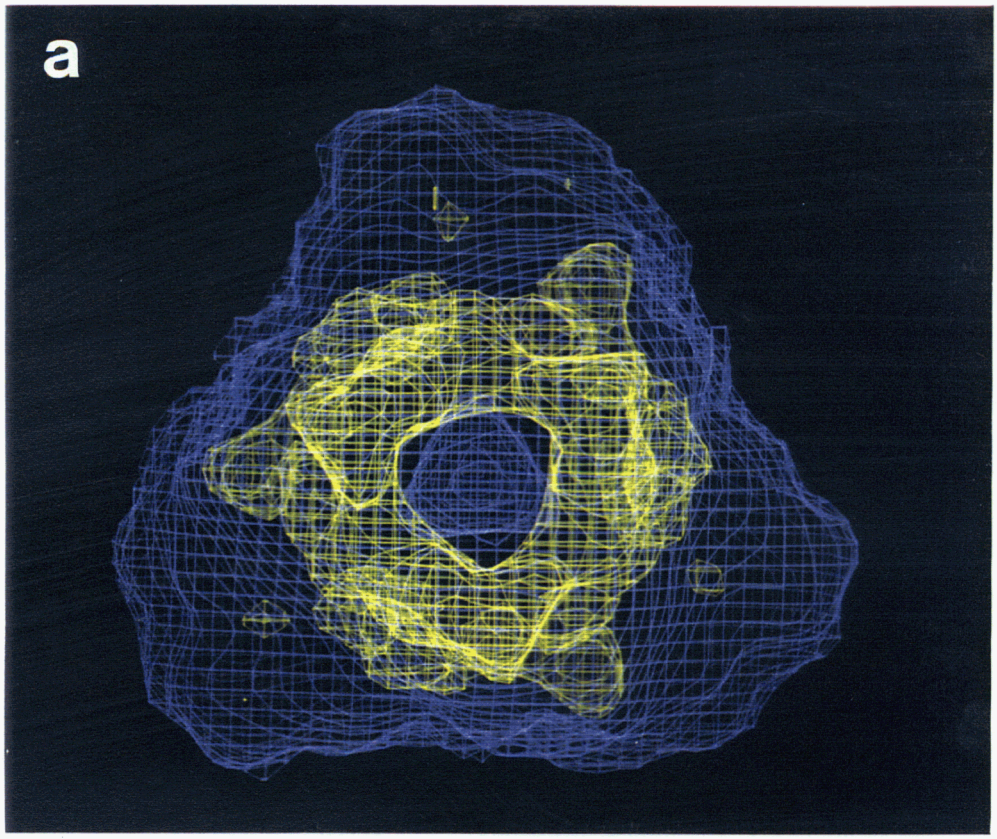
a

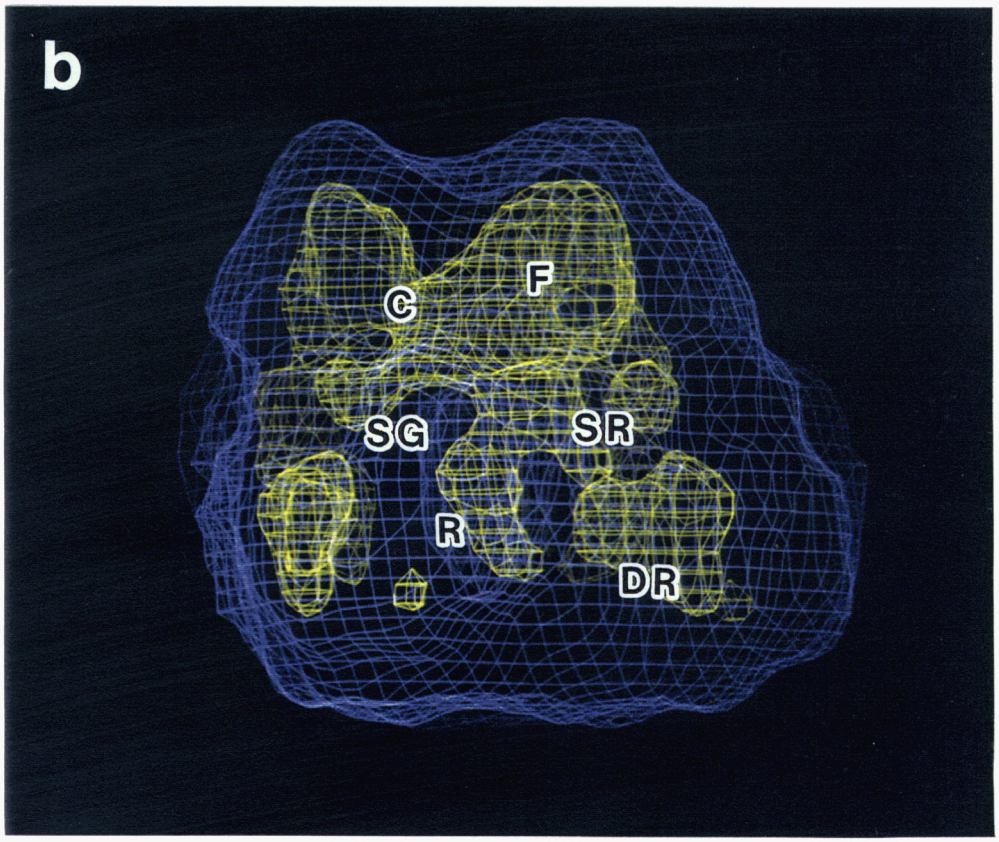
b
C
F
SG
SR
R
DR

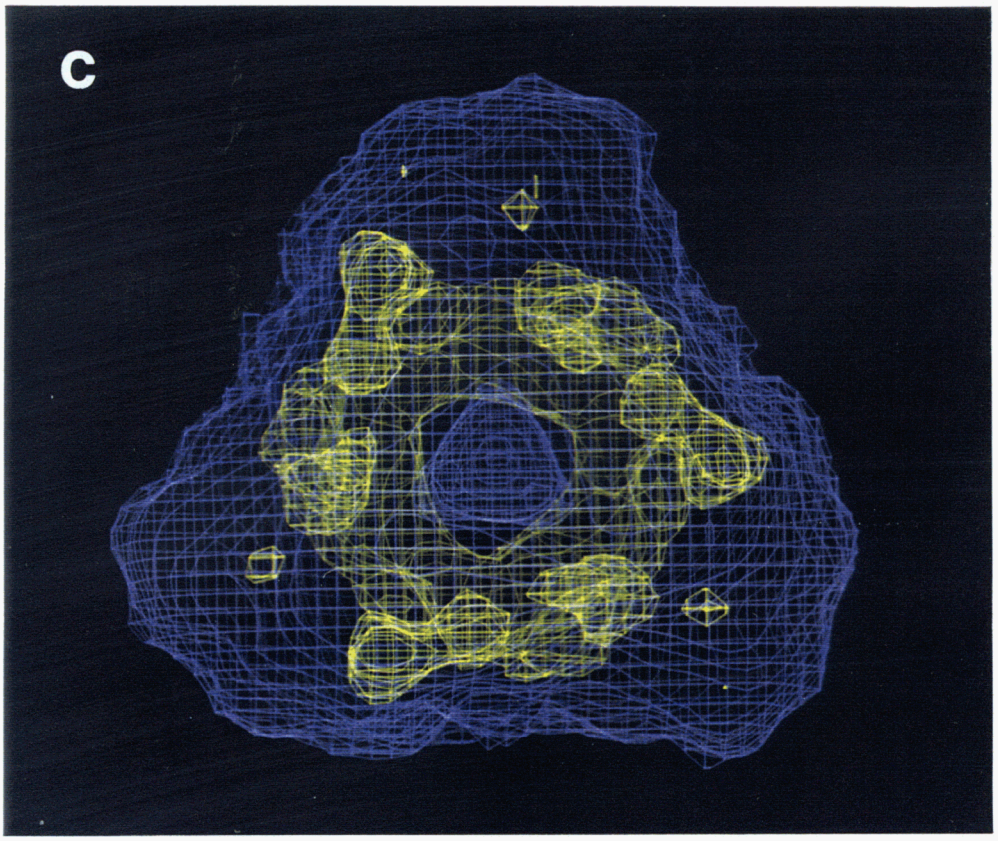

Figure 6. Fish-mesh representation of the triangular subunit after 3-fold averaging. Blue and yellow nets correspond to 2σ and 3σ, respectively. A view from the outer (a) and the inner side (c) of the tube. *b*, a view approximately perpendicular to the 3-fold axis. The domains divided into three parts along the 3-fold axis roughly and the 5 domains in high density region in Fig. 6*b* is indicated. The mesh size, 2Å.

axis normal to the helical axis. The triangular subunits side by side in the unit cell appear to be twisted a little to each other. The twisted interaction might be responsible for the tube formation because the subunits in the intact icosahedral virus particle are not twisted like this.

The cavity surrounded by the six triangular units is very similar to that found the small 2D crystal. The diameters of hexagonal cavities (2 nm) are nearly equal in the tube and the 2D crystal. A similar cavity is also observed in the virus particles (Lu *et al.*, 1995; Omura *et al.*, 1989; Uyeda & Shikata, 1982). Therefore, the local subunit packing of the tube is not very different from that of the intact virus particle except for the twist. As described in Chapter II-1, this cavity might be a candidate for a path by which solutes can enter and viral mRNA can leave the virus particle without any treatment (Kodama & Suzuki, 1973), as has been proposed for the core particles of rotavirus (Prasad *et al.*, 1988). Comparing the 3D structure of the icosahedral particle composed of P8 (unpublished) with that of the tube, orientation of the triangular units with respect to the shell wall is found to be the same. This triangular unit must correspond to that of the 2D crystal (Chapter II-1). Since the triangular unit of the 2D crystal is the trimer of P8, the triangular unit of the tubular crystal could be a trimer of P8. The interactions between the triangular units appear to occur around the side of the bottom domain. The most high density region near the side of bottom domain, is the longer rod of DS domain and the R domain. Although the longer rod of the DS domain and the R domain could face each other at the trimer-trimer interface, the spacing between them is about 20~ Å. This length is a little far for the formation of the helix-helix interaction. However, there is a possibility that the rod-like

structures are helices. We put the α-helices in the three-dimensional structure of the triangular unit (Fig. 7). The cylinder at the R domain tilts ~30° from the 3-fold axis. Predicted α-helix and β-sheet of P8 protein by Chou-Fasman method (Chou & Fasman, 1978) occupies 22.4% and 61.0%, respectively. The shortest α-helix is composed of 4 residues and the longest is 19 residues in predicted nine α-helix, that is, these α-helicies have diverse length from 6Å to 28.5Å. The cylinder representations of α-helicies corresponding to 9 residues, are put in Figure 7.

To form the icosahedral particle with the inner core, this bottom part could have critical role. The core shell composed of P3 proteins is also needed to form an intact virus particle (Takahashi *et al.*, 1994). The bottom part could play an important role in the interaction between the outer shell and the inner shell. In the process of the assembly of the virus particle, the arrangement of P8 protein like the tubular crystals might be utilized. Such polymorphic variants are observed in some kinds of virus, T4 phage, a virus associated with gastroenteritis (Holmes *et al.*, 1975; Kimura & Murakami, 1977), polyoma virus (Baker *et al.*, 1983).

As long as the discussion is limited at the top part, we can speculate the boundary between monomers in the triangular unit. The C domain that connects fin-like domain is a potential boundary because the C domain is the narrowest region in the large top part. Monomer-monomer interaction appears to be strong at the top part because most of high density region exists at the top part. As the β-sheet contents is very high, this fin-like domain might contain many β-sheets. The F domain might be used for keeping the trimer structure while the bottom part is used for trimer-trimer interaction. In terms of a function, the F domain could be important for the

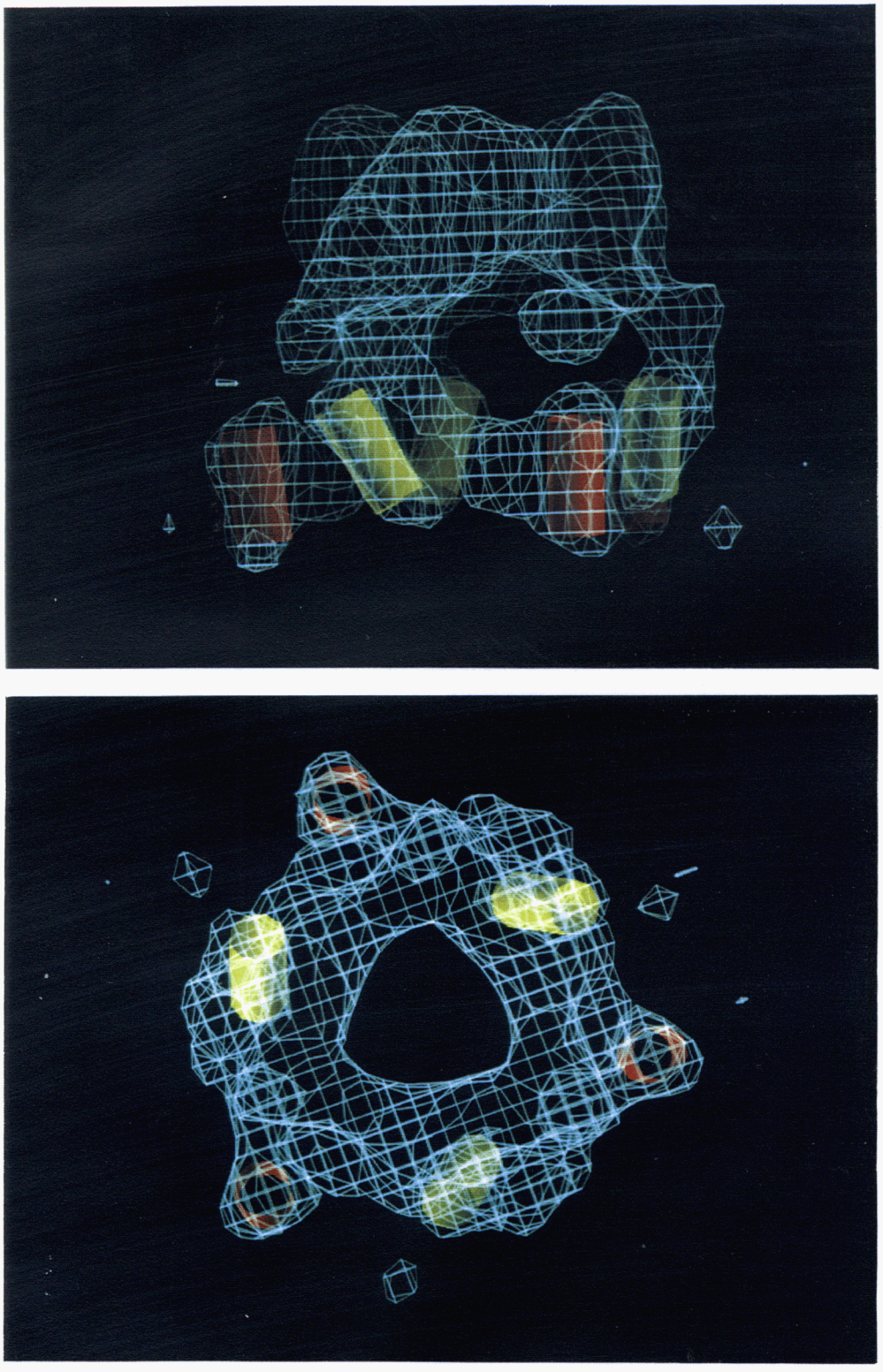

Figure 7. Fish-mesh representation of the triangular unit with cylindrical models of α-helices. a, view approximately perpendicular to the 3-fold axis normal to the herical axis of the tube. b, view from the outer tube. Light green nets correspond to 3σ. The mesh size, 2Å.

infection. Neutralizing antibodies can be raised against P8 protein (Omura, Unpublished). The interaction between antibodies and the P8 proteins must occur at the outside of the virus particle. Accordingly, the fin-like domain could be an antigenic determinant in the intact particle. As previously reported, antibodies against intact virus particles do not cross-react between RDV and RGDV (Omura et al., 1985), or between WTV and RDV (Liu & Black, 1978), suggesting that the domains with no identical amino acid sequences exposed outside. Since no identical regions are limited in small region (Noda *et al.*, 1991), we can narrow down candidates for antigenic determinant. Prediction of secondary structure of the residues between 361 and 369 showed that this region is neither α–helix nor β-sheet and so many β-sheets are predicted around that region. Therefore, this region might expose and become a hapten.

Consequently, multi-domain of the P8 trimer would be divided roughly into two parts. One is to keep the trimer structure as a unit; another is to work in the process of infection.

II-2.6 ACKNOWLEDGEMENTS

I am very grateful to Dr. Keiichi Namba and Koji Yonekura for leading me to a high resolution work. I would like to thank Kazuyoshi Murata for helping operate JEM-3000SFF. I also would like to thank Yafeng Zhu for sending purified samples several times. I am indebted to Katsumi Imada, Kaoru Mitsuoka and Michael Stowell for suggesting very important idea for data-analysis.

II-2.6 REFERENCE

Baker, T. S., Casper, D. L. D. & Murakami, W. T. (1983). Polyoma virus 'hexamer' tubes consist of paired pentamers. *Nature.* **303**, 446-448.

Böttcher, B., Wynne, S. A. & Crowther, R. A. (1997). Determination of the fold of the core protein of hepatitis B virus by electron cryomicroscopy. *Nature.* **386**, 88-91.

Chou, P. Y. & Fasman, G. D. (1978). Prediction of the secondary structure of proteins from their amino acid sequence. *Ann. Rev. Biochem.*, **47**, 25-76.

Conway, J. F., Cheng, N., Zlotnick, A., Wingfield, P. T., Stahl, S. J. & Steven, A. C. (1997). Visualization of a 4-helix bundle in the hepatitis B virus capsid by cryo-electron microscopy. *Nature.* **386**, 91-94.

Holmes, I. H., Boccardo, G., Estes, M. K., Furuichi, M. K., Hoshino, Y., Joklik, W. K., McCrae, M., Mertens, P. P. C., Milne, R. G., Samal, K. S. K., Shikata, E., Winton, J. R., Uyeda, I. & Nuss, D. L. (1995). Family Reoviridae. *Arch. Virol. Suppl.* **10**, 208-239.

Holmes, L. H., Ruck, B. J., Bishop, R. F. & Davidson, G. P. (1975). Infantile enteritis viruses: morphogenesis and morphology. *J. Virol.* **16**, 937-943.

Kimura, T. & Murakami, T. (1977). Tubular structures associated with acute nonbacterial gastroenteritis in young children. *Infection and Immunity* **17**, 157-160.

Kodama, T. & Suzuki, N. (1973). RNA polymerase activity in purified rice dwarf virus. *Ann. Phytopathol. Soc. Jpn.* **39**, 251-258.

Liu, H. Y. & Black, L. M. (1978). Neutralization of infectivity of potato

yellow dwarf virus and wound tumor virus assayed on vector-cell monolayers. *Phytopathology* **68**, 1243-1248.

Lu, G., Zhou, Z. H., Jakana, J., Deyou, C., Shengxiang, C., Xincheng, W., Xiaocheng, G. & Chiu, W (1995). Three-dimensional structure of rice dwarf virus by electron cryomicroscopy. *High Technol. Lett.* **1**, 1-4

Mimori, Y., Yamashita, I., Murata, K., Fujjiyoshi, Y., Yonekura, K., Toyoshima, C. & Namba, K. (1995). The structure of the R-type straight flagellar filament of *Salmonella* at 9Å resolution by electron cryomicroscopy. *J. Cell. Biol.* **249**, 69-87

Mizuno, H., Kano, H., Omura, T., Koizumi, M., Kondoh, M. & Tsukihara, T. (1991). Crystallization and preliminary X-ray study of a double shelled spherical virus, rice dwarf virus. *J. Mol. Biol.* **219**, 665-669.

Noda, H., Ishikawa, K., Hibino, H., Kato, H. & Omura, T. (1991). Nucleotide sequences of genome segment S8, encoding a capsid protein, and S10, encoding a 36K protein, of rice gall dwarf virus. *J. Gen. Virol.* **72**, 2837-2842

Omura, T., Ishikawa, K., Hirano, H., Ugaki, M., Minobe, Y., Tsuchizaki, T. & Kato, T. (1989). The outer capsid protein of rice dwarf virus is encoded by genome segment S8. *J. Gen. Virol.* **70**, 2759-2764

Omura, T., Minobe, Y., Matsuoka, M., Nozu, Y., Tsuchizaki, T. & Saito, Y. (1985). Location of structural proteins in particles of rice gall dwarf virus. *J. Gen. Virol.* **66**, 811-815.

Prasad, B. V. V., Wang, G. J., Clerx, J. P. M. & Chiu, W. (1988). Three-dimensional structure of rotavirus. *J. Mol. Biol.* **199**, 269-275.

Takahashi, Y., Tomiyama, M., Hibino, H. & Omura, T. (1994). Conserved primary structures in core capsid proteins and reassembly of core particles

and outer capsids between rice gall dwarf and rice dwarf phytoreoviruses. *J. Gen. Virol.* **75**, 269-275.

Toyoshima, C. & Unwin, N. (1988). Ion channel of acetylcholine receptor reconstructed from images of postsynaptic membranes. *Nature*. **336**, 247-250.

Toyoshima, C. & Unwin, N. (1990). Three dimensional structure of the acetylcholine receptor by cryoelectron microscopy and helical image reconstruction. *J. Cell. Biol.* **111**, 2623-2635

Uyeda, I. & Shikata, E. (1982). Ultrastructure of rice dwarf virus. *Ann. Phytopathol. Soc. Jpn.* **48**, 295-300

Zhu, Y., Hemmings, A. M., Iwasaki, K., Fujiyoshi, Y., Zhong, B., Yan, Jin., Isogau, M & Omura, T. (1997). Details of the arrangement of the outer capsid of rice dwarf phytoreovirus, as visualized by two-dimensionl crystallography. *J. Virol.* **71**, 8899-8901

Yan, J., Tomaru, M., Takahashi, A., Kimura, I., Hibino, H & Omura, T. (1996). P2 protein encoded by genome segment S2 of rice dwarf phtoreovirus is essential for virus infection. *Virology.* **224**, 539-541.

GENERAL DISCUSSION

The three-dimensional structure of integrin αIIbβ3 showed the characteristic structures of the head portion, at which the integrin might interact with fibrinogen. The interaction decide the relative position between αIIbβ3 and fibrinogen. Our result demonstrated that the tails were rigid except the tip of the them. These rigid portions, including transmembrane region, might play an roll in fixing the position of integrin on the membrane while interact with cytoskeleton. As a result, the relative position between platelets could be fixed, and, therefore, cytoskeleton in different platelets are arranged through the interaction between αIIbβ3 and fibrinogen.

The virus capsid protein, P8 was examined as an representative of proteins that build closed assemblies. Although the trimers twists in the tube, it is hardly possible for the trimers to twist each other. Therefore, this local twist might cause trimers to built tubular crystals. Presumably, the conformational change of the domain connecting the bottom part and other parts is caused by the variation of the solution containg P8. Such a slight change of the subunit determine the whole structure in this case.

In both case, the structure of the small region affects the whole structure. This is the most effective system to response the environmental change in the course of evolution.

ACKNOWLEDGEMENTS

I would like to thank Prof. Yoshinori Fujiyoshi and Prof. Toshio Yanagida for the opportunity to work in their laboratory. Prof. Yoshinori Fujiyoshi strengthened me and taught me what is a researcher. Prof. Toshio Yanagida always prepared good environment for my work, and urged me to go ahead.

I am also grateful to Dr. Toshihiro Omura. He supports all the study about P8.

I would like to thank Dr. Keiichi Namba, Dr. Koji Yonekura and Prof. Chikashi Toyoshima. They supplied very useful programs for helical image analysis.

Profs. Masakazu Kikuchi supported all the integrin work.

I would like to thank Dr. Holland Cheng for their grateful support in virus work.

Kazuyoshi Murata always arranged JEM-3000SFF electron microscope.

I am grateful to Dr.Kaoru Mitsuoka and Teruhisa Hirai for teaching me much things about computer.

I am very happy to work in this good environment.

Appendix

Programs developed for 3-fold averaging

I developed the programs on the base of *CCP4* programs. A density map is translated and rotated using *rotamap* of *CCP4* programs, and then a correlation between the shifted map and original map is calculated using *overlapmap* of *CCP4* programs.

1. *"matrix"* make a control file *"colseart.cnt"* for *rotamap* and *overlapmap*.

2. After executing *"colseart.cnt > colseart.out"*, you search *colseart.out* for the high correlation coefficient using *"peak_search.sh"*, which includes *"ext_correlation.awk"* and *"sort_pwak.awk"*. Then you can get the result in *"maxpeak.txt"*.

3. An original map and shifted map showing the highest coefficient are averaged.

peak_search.sh

```
awk -f ext_correlation.awk colseart.out > colseart.ext
awk -f sort_peak.awk colseart.ext > maxpeak.txt
```

ext_correlation.awk

```
/ROTA/{print $5,$6,$7}
/TRANS/{print $4,$5,$6}
/Total/{print $6,"\n"}
```

sort_peak.awk

```
BEGIN{RS=""}
{

   {
     total+=1
     RA[total]=$1
     RB[total]=$2
     RC[total]=$3
     TA[total]=$4
     TB[total]=$5
     TC[total]=$6
     col[total]=$7
    }
}
END{
 {
  for(i=1;i<=total-1;i++)
    for(j=i+1;j<=total;j++)
    {
    if(col[j]>col[i])
      {
        work=col[j]
        work2=RA[j]
        work3=RB[j]
        work4=RC[j]
        work5=TA[j]
        work6=TB[j]
        work7=TC[j]
        col[j]=col[i]
         RA[j]=RA[i]
         RB[j]=RB[i]
         RC[j]=RC[i]
         TA[j]=TA[i]
         TB[j]=TB[i]
         TC[j]=TC[i]
        col[i]=work
         RA[i]=work2
         RB[i]=work3
         RC[i]=work4
         TA[i]=work5
         TB[i]=work6
         TC[i]=work7
       }
    }
 }
{
for(i=1;i<=20;i++)
print i".",col[i],"\n",RA[i],RB[i],RC[i],TA[i],TB[i],TC[i]
}
}
```